

Discrete-Event Controller Synthesis for Autonomous Systems with Deep-Learning Perception Components

Radu Calinescu*, Calum Imrie*, Ravi Mangal†, Corina Păsăreanu†,
Misael Alpizar Santana*, and Gricel Vázquez*

We present DEEPDECS, a new method for the synthesis of correct-by-construction discrete-event controllers for autonomous systems that use deep neural network (DNN) classifiers for the perception step of their decision-making processes. Despite major advances in deep learning in recent years, providing safety guarantees for these systems remains very challenging. Our controller synthesis method addresses this challenge by integrating DNN verification with the synthesis of verified Markov models. The synthesised models correspond to discrete-event controllers guaranteed to satisfy the safety, dependability and performance requirements of the autonomous system, and to be Pareto optimal with respect to a set of optimisation criteria. We use the method in simulation to synthesise controllers for mobile-robot collision avoidance, and for maintaining driver attentiveness in shared-control autonomous driving.

Autonomous systems perceive the environment they operate in, and adapt their behaviour in response to changes in it. In application domains as diverse as medicine,^{1,2} finance³ and transportation,^{4,5} this perception is often performed using deep neural network (DNN) classifiers. The integration of deep-learning perception components into the control loop of autonomous systems used in such critical applications poses major challenges for their assurance.⁶ In particular, the long-established methods for formal software verification⁷ cannot be used to provide safety and performance guarantees for systems comprising both traditional software and deep-learning components. Newer verification methods developed specifically for DNNs focus on verifying robustness to changes in individual^{8,9} or clusters¹⁰ of DNN inputs. Therefore, they are equally unable to provide system-level guarantees for the controllers of autonomous systems with DNNs perception components.

Our paper presents DEEPDECS,^a a controller synthesis method that addresses this significant limitation. DEEPDECS employs a suite of DNN verification methods to quantify the *aleatory uncertainty* that the use of DNN perception components introduces in the control loop of the autonomous system under development. Discrete-event controllers guaranteed to satisfy the requirements of the autonomous system are then synthesised from a stochastic model that takes this uncertainty into account and leverages the high accuracy that DNNs can achieve for their verified inputs.

We start by introducing our DEEPDECS controller synthesis method, and its unique approach to exploiting both DNN and traditional-software verification techniques. Next, we describe the use of DEEPDECS to devise controllers for mobile-robot collision avoidance, and for using a combination of optical, audio and haptic alerts to improve driver attentiveness in vehicles provided with Level 3 automated driving systems.¹¹ Finally, we discuss DEEPDECS in the context of related work, and we propose directions for future research.

1 DEEPDECS controller synthesis

Overview. DEEPDECS uses a *parametric discrete-time Markov chain* (pDTMC) to model the design space of the controller under development. The uncertainty due to the use of a deep-learning perception component within the system to be controlled and, if applicable, the uncertainty inherent to the system and its environment are modelled by the probabilities of transition between the states of this pDTMC. Finally, the controller synthesis problem involves finding combinations of parameter values for which the Markov chain satisfies strict safety, dependability and performance constraints, and is Pareto-optimal with respect to a set of optimisation objectives. These constraints and optimisation objectives are formalised as probabilistic temporal logic formulae.

DEEPDECS derives the pDTMC underpinning its controller synthesis automatically from (i) DNN verification results that quantify the uncertainty due to the deep-learning perception component, and (i) an “ideal” pDTMC that models the behaviour of the controlled system assuming perfect perception (Figure 1a). The set of correct-by-construction, Pareto-optimal DEEPDECS controllers is then synthesised by applying a combination of probabilistic model checking and search techniques to the derived pDTMC. As shown in Figure 1b, each of these controllers operates by reacting to changes in the system, in the DNN outputs and, unique to DEEPDECS, in the results obtained through the online verification of each DNN input and prediction.

We detail each stage of the DEEPDECS approach below.

Stage 1: DNN uncertainty quantification. This section provides a brief introduction to DNN classifier verification, and describes the use of such verification techniques to quantify the aleatory uncertainty of DNN classifiers.

a) *Verification of DNN classifiers.* A K -class DNN classifier f_θ is a function, composed of linear and non-linear transformations, of the form

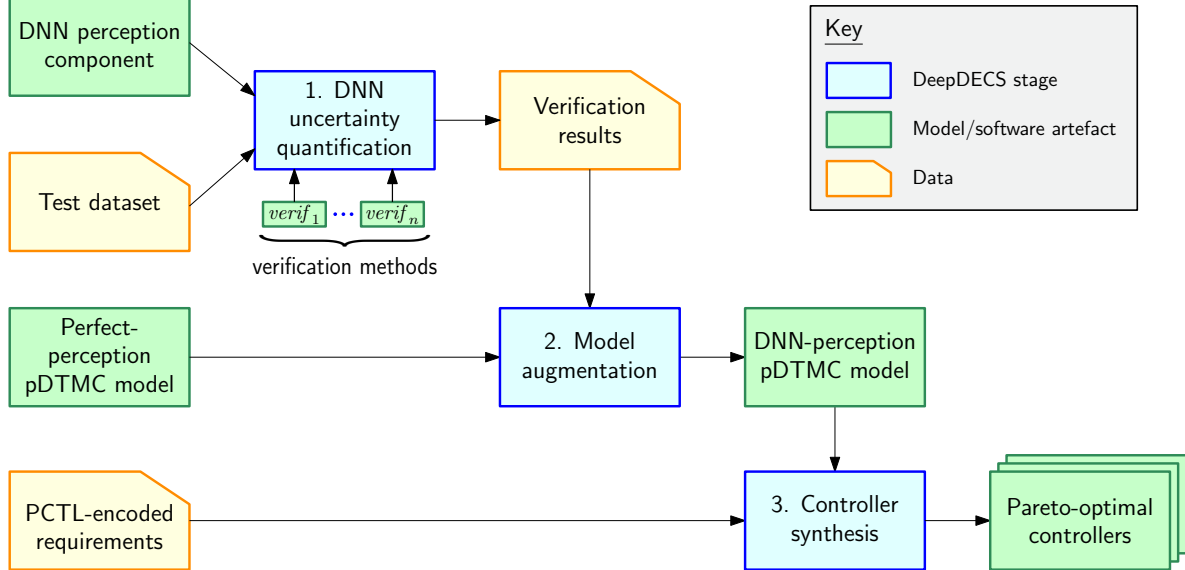
$$f_\theta: \mathbb{R}^d \rightarrow [K], \quad (1)$$

where $[K]$ denotes the set $\{1, \dots, K\}$, and θ refers to the

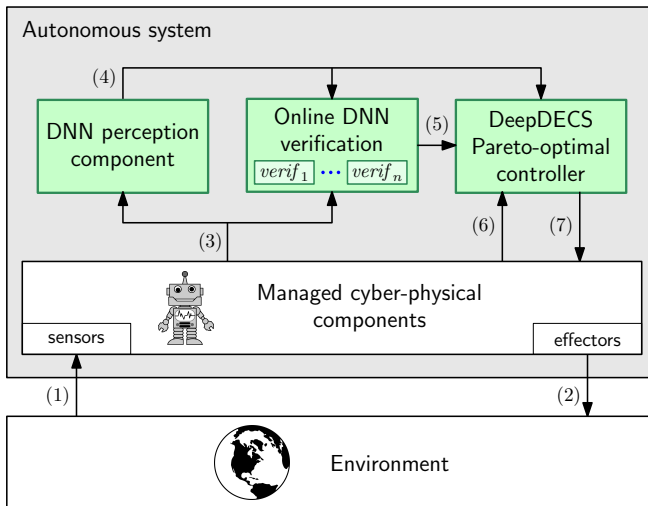
*Department of Computer Science, University of York, York, UK.

†Carnegie Mellon University, Silicon Valley, USA

^aDeep neural network perception Discrete-Event Controller Synthesis



(a) DEEPDECS generates discrete-event controllers aware of the uncertainty induced by the DNN perception component of an autonomous system in three stages. First, in a *DNN uncertainty quantification* stage, n verification methods are used to evaluate the DNN perception component over a test dataset representative for the operational design domain (ODD) of the autonomous system. The verification results provide a quantification of the DNN prediction uncertainty within the system ODD. Next, the *Model augmentation* stage uses these results—and an ideal-system pDTMC model that assumes perfect perception—to assemble a pDTMC system model that takes the DNN-induced uncertainty into account. Finally, the *Controller synthesis* stage uses this pDTMC model to synthesise a set of Pareto-optimal discrete-event controllers guaranteed to satisfy the PCTL-encoded requirements (constraints and optimisation objectives) of the system.



(b) The cyber-physical components of an autonomous system managed by a DEEPDECS controller monitor their environment through sensors (1) and perform actions that affect it through effectors (2). A DNN perception component uses a combination (3) of preprocessed sensor data and data about these managed components to classify the state of the environment (4). The n verification methods used for the DEEPDECS controller synthesis are also applied to the classification (4) and the DNN input (3) that produced it. Using the online DNN verification results (5) alongside the classification (4) and additional state information (6) obtained directly from the managed cyber-physical components, the DEEPDECS controller updates (7) the controllable parameters of these components in line with the system requirements.

Figure 1: DEEPDECS controller synthesis (a), and deployment (b)

weights or parameter values that characterize the linear transformations. As the results presented in this article are oblivious to the internal details of DNNs, we will by default omit the subscript θ , and treat f as a black-box function.

DNN classifiers are learnt from data, and are not guaranteed to always classify their input correctly. DNN verification techniques can help assess the quality of a classifier for a

given input. A verification technique has the general form

$$verif : (\mathbb{R}^d \rightarrow [K]) \times \mathbb{R}^d \rightarrow \mathbb{B}, \quad (2)$$

such that, for a classifier $f \in \mathbb{R}^d \rightarrow [K]$ and an input $x \in \mathbb{R}^d$, $verif(f, x) = \text{true}$ if the verification technique deems the DNN f likely to classify the input x correctly, and $verif(f, x) = \text{false}$ otherwise. Two examples of simple DNN verification techniques

(which we use to evaluate DEEPDECS later in the article) are:

1. *Model confidence threshold*—A K -class DNN classifier is practically implemented as a function of type $\mathbb{R}^d \rightarrow [0,1]^K$, with each input $x \in \mathbb{R}^d$ first mapped to a discrete probability distribution $\delta(x) = (p_1, p_2, \dots, p_K)$ over the K classes, and the class corresponding to the highest probability is chosen as the classifier prediction. The probability associated with a class can be interpreted as estimating the probability that the class is the *true* label of x . While it has been observed that classifiers may not be well-calibrated, i.e., the estimated correctness probabilities may be far from the true probabilities, a number of methods have been proposed to calibrate DNN classifiers.¹² Assuming that a classifier is well-calibrated using one of these methods, a simple DNN verification technique is to check whether the estimate correctness probability for an input x is greater than a fixed threshold τ for the class with the highest probability:

$$\text{verif}_1(f,x) = \begin{cases} \text{true, if } \max_{i=1}^K p_i \geq \tau \\ \text{false, otherwise} \end{cases} \quad (3)$$

2. *Local robustness certification*¹³—A DNN classifier f is ϵ -locally robust at an input x if perturbations within a small distance $\epsilon > 0$ from x (measured using the ℓ_2 metric) do not lead to a change in the classifier prediction. Accordingly, the local robustness verifier is defined by

$$\text{verif}_2(f,x) = \begin{cases} \text{true, if } \forall x' \in \mathbb{R}^d. \|x - x'\|_2 \leq \epsilon \\ \qquad \qquad \qquad \implies f(x) = f(x') \\ \text{false, otherwise} \end{cases} \quad (4)$$

for any input $x \in \mathbb{R}^d$.

b) *Quantification of DNN perception uncertainty*. The use of DNN perception introduces aleatory uncertainty into the autonomous system since DNNs are not guaranteed to predict accurately on all inputs. In the first DEEPDECS stage, we use a mechanism that relies on DNN verification techniques to empirically quantify the uncertainty of the DNN outcomes.

Let $X \subset \mathbb{R}^d$ be a *representative test dataset* for the DNN classifier (1), i.e., a set of classifier inputs that reflects the inputs that the autonomous system using the DNN will encounter in its ODD. For any test input $x \in X$, let $f^*(x) \in [K]$ be the label (i.e., the true class) of x , which is known since X is a test dataset.

DEEPDECS uses $n \geq 0$ DNN verification techniques $\text{verif}_1, \text{verif}_2, \dots, \text{verif}_n$ to identify subsets of X for which the classifier is likely to achieve higher accuracy than for the entire set X .^b We use the n verification methods to partition the test dataset X into 2^n subsets comprising inputs x with the same verification results.^c Formally, for a DNN classifier f and any $v = (v_1, v_2, \dots, v_n) \in \mathbb{B}^n$, we define the test data subset

$$X_v = \{x \in X \mid \text{verif}(f,x) = v\}, \quad (5)$$

^bNote that DEEPDECS is also applicable in the special case when $n=0$, i.e., when no verification techniques is used.

^cAs typical values for n are $n=1,2,3$, there will only be a small number of such subsets.

where $\text{verif}(f,x) = (\text{verif}_1(f,x), \text{verif}_2(f,x), \dots, \text{verif}_n(f,x))$. We use each of these test data subsets to define a $K \times K$ confusion matrix \mathcal{C}_v such that, for any $k, k' \in [K]$, the element in row k and column k' of this matrix is given by the number of inputs from X_v with true class k that the DNN classifies as belonging to class k'

$$\mathcal{C}_v[k,k'] = \#\{x \in X_v \mid f^*(x) = k \wedge f(x) = k'\}, \quad (6)$$

where, for any set A , $\#A$ denotes its cardinality.

As the test dataset X is representative of the DNN inputs that the system encounters in operation, we henceforth assume that the probability that a class- k input x satisfies $\text{verif}(f,x) = v$ and is (mis)classified by the DNN as belonging to class k' is given by:^d

$$\begin{aligned} p_{kk'v} &= \Pr(f(x) = k' \wedge \text{verif}(f,x) = v \mid f^*(x) = k) \\ &= \frac{\mathcal{C}_v[k,k']}{\sum_{v' \in \mathbb{B}^n} \sum_{k'' \in [K]} \mathcal{C}_{v'}[k,k'']}. \end{aligned} \quad (7)$$

Stage 2: Model augmentation. This section provides a brief introduction to pDTMCs, defines the discrete-event controller synthesis problem, and presents the DEEPDECS theory underlying the generation of pDTMCs that model the behaviour of, and support the synthesis of controllers for, autonomous systems with deep-learning perception components.

a) *Discrete-time Markov chains.* DEEPDECS models the design space (i.e., the possible variants) for the controller of an autonomous system as a pDTMC augmented with *rewards*.

Definition 1. A *reward-augmented discrete-time Markov chain (DTMC)* over a set of atomic propositions AP is a tuple

$$\mathcal{M} = (S, s_0, P, L, R), \quad (8)$$

where $S \neq \emptyset$ is a finite set of states; $s_0 \in S$ is the initial state; $P : S \times S \rightarrow [0,1]$ is a transition probability function such that, for any states $s, s' \in S$, $P(s, s')$ gives the probability of transition from state s to state s' and $\sum_{s' \in S} P(s, s') = 1$; $L : S \rightarrow 2^{AP}$ is a labelling function that maps every state $s \in S$ to the atomic propositions from AP that hold in that state; and R is a set of reward structures, i.e., function pairs (ρ, ι) that associate non-negative values with the pDTMC states and transitions:

$$\rho : S \rightarrow \mathbb{R}_{\geq 0}, \iota : S \times S \rightarrow \mathbb{R}_{\geq 0}. \quad (9)$$

When (8) includes unknown transition probabilities and/or reward values, the DTMC is termed *parametric*.

Definition 2. A *reward-augmented parametric discrete-time Markov chain* is a DTMC (8) comprising one or several transition probabilities and/or rewards that are specified as rational functions^e over a set of continuous variables.¹⁴

DEEPDECS uses *probabilistic computation tree logic* (PCTL)^{15,16} extended with rewards¹⁷ to quantify the safety, dependability and performance properties of an autonomous system whose controller design space is modelled as a pDTMC.

^dFormally, this results holds as $\#X \rightarrow \infty$.

^ei.e., functions that can be written as fractions whose numerators and denominators are polynomial functions, e.g., $1-p$ or $\frac{1-p_1}{p_2}$

Definition 3. State PCTL formulae Φ and path PCTL formulae Ψ over an atomic proposition set AP , and PCTL reward formulae Φ_R over a reward structure (9) are defined by the grammar:

$$\begin{aligned}\Phi &::= \text{true} \mid \alpha \mid \Phi \wedge \Phi \mid \neg \Phi \mid \mathcal{P}_{\sim p}[\Psi] \\ \Psi &::= X\Phi \mid \Phi \text{U} \Phi \mid \Phi \text{U}^{\leq k} \Phi \\ \Phi_R &::= \mathcal{R}_{\sim r}[\mathcal{C}^{\leq k}] \mid \mathcal{R}_{\sim r}[\mathcal{F} \Phi]\end{aligned}\quad (10)$$

where $\alpha \in AP$ is an atomic proposition, $\sim \in \{\geq, >, <, \leq\}$ is a relational operator, $p \in [0, 1]$ is a probability bound, $r \in \mathbb{R}_0^+$ is a reward bound, and $k \in \mathbb{N}_{>0}$ is a timestep bound.

The PCTL semantics^{15–17} is defined using a satisfaction relation \models over the states of a DTMC. Given a state s of a DTMC \mathcal{M} , $s \models \Phi$ means ‘ Φ holds in state s ’, and we have: **always** $s \models \text{true}$; $s \models \alpha$ iff $\alpha \in L(s)$; $s \models \neg \Phi$ iff $\neg(s \models \Phi)$; and $s \models \Phi_1 \wedge \Phi_2$ iff $s \models \Phi_1$ and $s \models \Phi_2$. The **time-bounded until formula** $\Phi_1 \text{U}^{\leq k} \Phi_2$ holds for a **path** (i.e., sequence of DTMC states $s_0 s_1 s_2 \dots$ such that $P(s_i, s_{i+1}) > 0$ for all $i > 0$) iff Φ_1 holds in the first $i < k$ path states and Φ_2 holds in the $(i+1)$ -th path state; and the **unbounded until formula** $\Phi_1 \text{U} \Phi_2$ removes the bound k from the time-bounded until formula. The **next formula** $X\Phi$ holds if Φ is satisfied in the next state. The semantics of the probability \mathcal{P} and reward \mathcal{R} operators are defined as follows: $\mathcal{P}_{\sim p}[\Psi]$ specifies that the probability that paths starting at a chosen state s satisfy a path property Ψ is $\sim p$; $\mathcal{R}_{\sim r}[\mathcal{C}^{\leq k}]$ holds if the expected cumulated reward up to time-step k is $\sim r$; and $\mathcal{R}_{\sim r}[\mathcal{F} \Phi]$ holds if the expected reward cumulated before reaching a state satisfying Φ is $\sim r$. Replacing $\sim p$ (or $\sim r$) from (10) with ‘=?’ specifies that the calculation of the probability (or reward) is required. We use the shorthand notation $\text{pmc}(\Phi, \mathcal{M})$ and $\text{pmc}(\Phi_R, \mathcal{M})$ for these quantities computed for the initial state s_0 of \mathcal{M} .

b) Discrete-event controller synthesis problem. To distinguish between different concerns of the autonomous system to be controlled, DEEPDECS organises each state s of the perfect-perception pDTMC model from Figure 1 into a tuple

$$s = (z, k, t, c), \quad (11)$$

where $z \in Z$ models the (internal) state of the system, $k \in [K]$ models the state of the environment, $c \in C$ models the control parameters of the system, and $t \in [3]$ is a “turn” flag. This flag indicates which elements of (11) can change in each pDTMC state:

$$\begin{aligned}\forall s = (z, k, t, c), s' = (z', k', t', c') \in S: \\ ((t=1 \wedge P(s, s') > 0) \implies k' = k \wedge c' = c \wedge t' < 3) \wedge \\ ((t=2 \wedge P(s, s') > 0) \implies z' = z \wedge c' = c \wedge t' = 3) \wedge \\ ((t=3 \wedge P(s, s') > 0) \implies z' = z \wedge k' = k \wedge t' = 1).\end{aligned}\quad (12)$$

We partition the pDTMC state set into states in which the system can change, states in which the environment can change, and states in which it is the controller’s “turn” to act for simplicity, and without loss of generality; the three types of states can be easily collapsed into one.

Finally, we assume that the outgoing transition probabilities from states $(z, k, 3, c) \in S$ are controller parameters that need to be determined and are given by

$$x_{zkc} = P((z, k, 3, c), (z, k, 1, c')) \quad (13)$$

for all $c' \in C$, where $x_{zkc} \in \{0, 1\}$ for **deterministic controllers** or $x_{zkc} \in [0, 1]$ for **probabilistic controllers**, and $\sum_{c' \in C} x_{zkc} = 1$.

Figure 2a shows the general format of a DEEPDECS perfect-perception pDTMC model, defined in the high-level modelling language of the PRISM model checker.¹⁸ In this language, the model of a system is specified by the parallel composition of a set of *modules*. The state of a *module* is given by a set of finite-range local variables, and its state transitions are specified by probabilistic guarded commands that change these variables:

$$[\text{action}] \text{ guard} \rightarrow e_1 : \text{update}_1 + e_2 : \text{update}_2 + \dots + e_m : \text{update}_N; \quad (14)$$

In this command, *guard* is a boolean expression over the variables of all modules. If *guard* evaluates to true, the arithmetic expression e_i , $i \in [m]$, gives the probability with which the update_i change of the module variables occurs. When *action* is present, all modules comprising commands with this *action* have to *synchronise*, i.e., to perform one of these commands simultaneously.

With this notation introduced so far, the *controller synthesis problem for the perfect-perception system* is to find the set of Pareto-optimal parameters (13) which ensure that the pDTMC satisfies $n_1 \geq 0$ PCTL-encoded *constraints* of the form in (10),

$$C_i ::= \Phi_i \mid \Phi_{Ri} \quad (15)$$

and Pareto-optimises $n_2 \geq 1$ PCTL-encoded *objectives* of the form

$$\begin{aligned}O_j ::= \text{maximise } \text{pmc}(\Phi_j, \mathcal{M}) \mid \text{minimise } \text{pmc}(\Phi_j, \mathcal{M}) \\ \text{maximise } \text{pmc}(\Phi_{Rj}, \mathcal{M}) \mid \text{minimise } \text{pmc}(\Phi_{Rj}, \mathcal{M})\end{aligned}\quad (16)$$

where $i \in [n_1]$ and $j \in [n_2]$.

c) Model augmentation. The controller of an autonomous system with deep-learning perception does not have access to the true value k of the environment state from (11). Instead, DEEPDECS controllers need to operate with an estimate $\hat{k} \in [K]$ of this true value, and with the results $v = (v_1, v_2, \dots, v_n) \in \mathbb{B}^n$ of $n \geq 0$ verification techniques (2) applied to the DNN and its input that produced the estimate \hat{k} . As such, the states \hat{s} of a DEEPDECS *DNN-perception pDTMC model*

$$\hat{\mathcal{M}} = (\hat{S}, \hat{s}_0, \hat{P}, \hat{L}, \hat{R}) \quad (17)$$

are tuples that extend (11) with \hat{k} and v :

$$\hat{s} = (z, k, \hat{k}, v, t, c). \quad (18)$$

The derivation of the DEEPDECS DNN-perception pDTMC from the perfect-perception pDTMC is shown in Figure 2b. To provide a formal definition of this derivation, we use the notation $s(\hat{s}) = (z, k, t, c)$ to refer to the element from $Z \times [K] \times [3] \times C$ that corresponds to a generic element corresponding to $\hat{s} \in Z \times [K]^2 \times \mathbb{B}^n \times [3] \times C$. With this notation, the components of the pDTMC $\hat{\mathcal{M}}$ are obtained from the perfect-perception pDTMC $\mathcal{M} = (S, s_0, P, L, R)$ of the same autonomous system and the probabilities (7) as follows:

$$\hat{S} = \{\hat{s} \in Z \times [K]^2 \times \mathbb{B}^n \times [3] \times C \mid s(\hat{s}) \in S\}; \quad (19)$$

```

dtmc

module ManagedComponents
  z : Z init z0;
  [action1] t=1 ∧ guard1Z(z,c) → e11Z:(z'=z11) + ... + e1N1Z:(z'=z1N1);
  [action2] t=1 ∧ guard2Z(z,c) → e21Z:(z'=z21) + ... + e2N2Z:(z'=z2N2);
  ...
endmodule

module Environment
  k : [K] init k0;
  [monitor] t=2 ∧ guard1K(z,k) → e11K:(k'=1) + ... + e1KK:(k'=K);
  [monitor] t=2 ∧ guard2K(z,k) → e21K:(k'=1) + ... + e2KK:(k'=K);
  ...
endmodule

module PerfectPerceptionController
  c : C init c0;
  [decide] t=3 ∧ guard1C(z,k,c) → ∑c' ∈ C (xzkcc':(c'=c'));
  [decide] t=3 ∧ guard2C(z,k,c) → ∑c' ∈ C (xzkcc':(c'=c'));
  ...
endmodule

module Turn
  t : [1..3] init 1;
  [actionα] true → 1:(t'=2);
  [actionβ] true → 1:(t'=2);
  ...
  [monitor] true → 1:(t'=3);
  [decide] true → 1:(t'=1);
endmodule

```

(a) A DEEPDECS perfect-perception pDTMC comprises four modules. The module **ManagedComponents** models the controlled components of the system by specifying how their state z changes as a result of set of actions $Act = \{\text{action}_1, \text{action}_2, \dots\}$ performed when the value of the turn flag is $t=1$; the guards of this module depend only on the state z of the components and the control parameters c . The module **Environment** models how the evolving state of environment k changes when observed through monitoring when the value of the turn flag is $t=2$; the guards of this module depend only on the state z of the system components and on the current state k of the environment. The controller decisions are defined by the **PerfectPerceptionController** module with parameters (13). Finally, the module **Turn** sets the turn flag to $t=2$ when, after specific actions $\text{action}_\alpha, \text{action}_\beta, \dots \in Act$, it is the monitor's turn to observe the environment, sets the turn flag to $t=3$ after each such **monitor** action to trigger a controller **decision**, and restores the turn flag to $t=1$ immediately after that to enable the controlled system components to react to the new control parameters of the system.

```

dtmc

module ManagedComponents
  z : Z init z0;
  [action1] t=1 ∧ guard1Z(z,c) → e11Z:(z'=z11) + ... + e1N1Z:(z'=z1N1);
  [action2] t=1 ∧ guard2Z(z,c) → e21Z:(z'=z21) + ... + e2N2Z:(z'=z2N2);
  ...
endmodule

module EnvironmentWithDNNPerception
  k : [K] init k0;
   $\hat{k}$  : [K] init k0;
  v :  $\mathbb{B}^n$  init (true,true,...,true);
  [monitor] t=2 ∧ guard1K(z,k) → ∑k' ∈ [K] ∑v' ∈  $\mathbb{B}^n$  (e11KK p1k'v':(k'=1 &  $\hat{k}'=k'$  & v=v'));
  ...
  [monitor] t=2 ∧ guard2K(z,k) → ∑k' ∈ [K] ∑v' ∈  $\mathbb{B}^n$  (e21KK p2k'v':(k'=2 &  $\hat{k}'=k'$  & v=v'));
  ...
endmodule

module DNNPerceptionController
  c : C init c0;
  [decide] t=3 ∧ guard1C(z, $\hat{k}$ ,c) ∧ v=(false,false,...,false) → ∑c' ∈ C (xzkvc':(c'=c'));
  ...
  [decide] t=3 ∧ guard1C(z, $\hat{k}$ ,c) ∧ v=(true,true,...,true) → ∑c' ∈ C (xzkvc':(c'=c'));
  [decide] t=3 ∧ guard2C(z, $\hat{k}$ ,c) ∧ v=(false,false,...,false) → ∑c' ∈ C (xzkvc':(c'=c'));
  ...
  [decide] t=3 ∧ guard2C(z, $\hat{k}$ ,c) ∧ v=(true,true,...,true) → ∑c' ∈ C (xzkvc':(c'=c'));
endmodule

module Turn
  t : [1..3] init 1;
  [actionα] true → 1:(t'=2);
  [actionβ] true → 1:(t'=2);
  ...
  [monitor] true → 1:(t'=3);
  [decide] true → 1:(t'=1);
endmodule

```

(b) DEEPDECS DNN-perception pDTMC model obtained by performing the highlighted modification in the perfect-perception pDTMC from Figure 2a. As a consequence of using a DNN to perceive the true environment state k , the **DNNPerceptionController** does not have access to its value; instead, it needs to rely on its classification \hat{k} and on the verification result v , respectively. The **EnvironmentWithDNNPerception** module continues to track the ground truth k (necessary to establish the true safety, energy consumption, and other key properties of the system). Additionally, this module uses the DNN uncertainty quantification probabilities (7) to model the evolution of the DNN output \hat{k} and the online DNN verification result v associated with this output. The modules **ManagedComponents** and **Turn** are unchanged.

Figure 2: Perfect-perception and DNN-perception DEEPDECS pDTMC models

$$\hat{s}_0 = (z_0, k_0, k_0, \text{true}, \dots, \text{true}, t_0, c_0), \quad (20)$$

where $(z_0, k_0, t_0, c_0) = s_0$; and, for any states $\hat{s} = (z, k, \hat{k}, v, t, c)$, $\hat{s}' = (z', k', \hat{k}', v', t', c') \in \hat{S}$,

$$\hat{P}(\hat{s}, \hat{s}') = \begin{cases} P(s(\hat{s}), s(\hat{s}')), & \text{if } t=1 \wedge (\hat{k}', v') = (\hat{k}, v) \\ P(s(\hat{s}), s(\hat{s}')) \cdot p_{k'\hat{k}'v'}, & \text{if } t=2 \\ x_{z\hat{k}vc'}, & \text{if } t=3 \wedge (z', k', \hat{k}', v', t') \\ & = (z, k, \hat{k}, v, 1) \\ 0, & \text{otherwise} \end{cases} \quad (21)$$

where $x_{z\hat{k}vc'}$ are controller parameters associated with state

pairs $((z, k, \hat{k}, v, 3, c), (z, k, \hat{k}, v, 3, c')) \in \hat{S}^2$ such that $x_{z\hat{k}vc'} \in \{0, 1\}$ for deterministic controllers or $x_{z\hat{k}vc'} \in [0, 1]$ for probabilistic controllers, and $\sum_{c' \in C} x_{z\hat{k}vc'} = 1$. Finally, for any state $\hat{s} \in \hat{S}$,

$$\hat{L}(\hat{s}) = L(s(\hat{s})), \quad (22)$$

and

$$\begin{aligned} \hat{R} = & \{(\hat{\rho}, \hat{\iota}) \in (\hat{S} \rightarrow \mathbb{R}_{\geq 0}) \times (\hat{S} \times \hat{S} \rightarrow \mathbb{R}_{\geq 0}) \mid \\ & \exists (\rho, \iota) \in R: (\forall \hat{s} \in \hat{S}: \hat{\rho}(\hat{s}) = \rho(s(\hat{s}))) \wedge \\ & (\forall \hat{s}, \hat{s}' \in \hat{S}: \hat{\iota}(\hat{s}, \hat{s}') = \iota(s(\hat{s}), s(\hat{s}')))\} \end{aligned} \quad (23)$$

The following result shows that the DEEPDECS module augmentation produces a valid pDTMC.

Theorem 1. *The tuple (17) with the elements defined by (19)–(23) is a valid pDTMC that satisfies the following variant of (12):*

$$\begin{aligned} \forall \hat{s} = (z, k, \hat{k}, v, t, c), \hat{s}' = (z', k', \hat{k}', v', t', c') \in \hat{S}: \\ ((t=1 \wedge P(\hat{s}, \hat{s}') > 0) \implies (k', \hat{k}', v', c') = (k, \hat{k}, v, c) \wedge t' < 3) \wedge \\ ((t=2 \wedge P(\hat{s}, \hat{s}') > 0) \implies (z', c') = (z, c) \wedge t' = 3) \wedge \\ ((t=3 \wedge P(\hat{s}, \hat{s}') > 0) \implies (z', k', \hat{k}', v') = (z, k, \hat{k}, v) \wedge t' = 1). \end{aligned} \quad (24)$$

Proof. To demonstrate that (17) is a valid pDTMC, we need to show that, for any state $\hat{s} = (z, k, \hat{k}, v, t, c) \in \hat{S}$, $\sum_{\hat{s}' \in \hat{S}} \hat{P}(\hat{s}, \hat{s}') = 1$. We prove this and property (24) for each value of $t \in [3]$.

For $t=1$, (21) implies that $\hat{P}(\hat{s}, \hat{s}') > 0$ only for states $\hat{s}' = (z', k', \hat{k}, v, t', c') \in \hat{S}$, so

$$\begin{aligned} \sum_{\hat{s}' \in \hat{S}} \hat{P}(\hat{s}, \hat{s}') &= \sum_{(z', k', \hat{k}, v, t', c') \in \hat{S}} \hat{P}(\hat{s}, \hat{s}') \\ &= \sum_{(z', k', \hat{k}, v, t', c') \in \hat{S}} P((z, k, 1, c), (z', k', t', c')) \\ &= \sum_{(z', k', t', c') \in S} P((z, k, 1, c), (z', k', t', c')) = 1, \end{aligned}$$

as the last sum adds up all outgoing transition probabilities of state (z', k', t', c') from the perfect-perception pDTMC \mathcal{M} . Consider now any $\hat{s}' = (z', k', \hat{k}', v', t', c') \in \hat{S}$ such that $\hat{P}(\hat{s}, \hat{s}') > 0$. We already noted that this requires $\hat{k}' = \hat{k} \wedge v' = v$. Additionally, since $\hat{P}(\hat{s}, \hat{s}') = P((z, k, 1, c), (z', k', t', c'))$, (12) implies that $k' = k \wedge c' = c \wedge t' < 3$, as required by (24).

For $t=2$, we have

$$\begin{aligned} \sum_{\hat{s}' \in \hat{S}} \hat{P}(\hat{s}, \hat{s}') &= \sum_{(z', k', \hat{k}', v', t', c') \in \hat{S}} \left(\hat{P}(\hat{s}, \hat{s}') p_{k' \hat{k}' v'} \right) \\ &= \sum_{(z', k', t', c') \in S} \left(P((z, k, 2, c), (z', k', t', c')) \cdot \sum_{(\hat{k}', v')' \in [K] \times \mathbb{B}^n} p_{k' \hat{k}' v'} \right) \\ &= \sum_{(z', k', t', c') \in S} (P((z, k, 2, c), (z', k', t', c')) \cdot 1) = 1. \end{aligned}$$

Consider again a generic $\hat{s}' = (z', k', \hat{k}', v', t', c') \in \hat{S}$ such that $\hat{P}(\hat{s}, \hat{s}') > 0$. Since $\hat{P}(\hat{s}, \hat{s}') = P((z, k, 2, c), (z', k', t', c')) \cdot p_{k' \hat{k}' v'}$, (12) implies that $(z', c') = (z, c) \wedge t' = 3$.

Finally, for $t=3$, we have $\sum_{\hat{s}' \in \hat{S}} \hat{P}(\hat{s}, \hat{s}') = \sum_{c' \in C} x_{z \hat{k} v c'} = 1$ and the property (24) is explicitly stated in (21). \square

Importantly, the next result shows that the controller decisions do not depend on the true state k of the environment.

Theorem 2. *For any $(z, k_1, \hat{k}, v, 3, c), (z, k_2, \hat{k}, v, 3, c) \in \hat{S}$ and any control parameters $c' \in C$,*

$$\begin{aligned} \hat{P}((z, k_1, \hat{k}, v, 3, c), (z, k_1, \hat{k}, v, 1, c')) \\ = \hat{P}((z, k_2, \hat{k}, v, 3, c), (z, k_2, \hat{k}, v, 1, c')). \end{aligned} \quad (25)$$

Proof. According to definition (21), both transition probabilities from (25) are equal to $x_{z \hat{k} v c'}$. \square

Finally, the following theorem and its corollaries prove that for each (probabilistic) discrete-event controller that satisfies constraints (15) and Pareto-optimises objectives (16) for the autonomous system with DNN perception there is an equivalent (probabilistic) discrete-event controller for the autonomous system with perfect perception, but the converse does not hold.

Theorem 3. *Let \underline{x} and $\hat{\underline{x}}$ be valid instantiations of the perfect-perception controller parameters $\{x_{z k c c'} \in [0, 1] \mid (\exists k \in [K], (z, k, 3, c) \in S) \wedge c' \in C\}$ from (13) and of the DNN-perception controller parameters $\{x_{z \hat{k} v c c'} \in [0, 1] \mid (\exists k \in [K], (z, k, \hat{k}, v, 3, c) \in \hat{S}) \wedge c' \in C\}$ from (21), respectively. Also, let $\mathcal{M}_{\underline{x}}$ and $\hat{\mathcal{M}}_{\hat{\underline{x}}}$ be the instances of the perfect-perception pDTMC \mathcal{M} and DNN-perception pDTMC $\hat{\mathcal{M}}$ corresponding to the controller parameters \underline{x} and $\hat{\underline{x}}$, respectively. With this notation, we have*

$$pmc(\Phi, \hat{\mathcal{M}}_{\hat{\underline{x}}}) = pmc(\Phi, \mathcal{M}_{\underline{x}}), \quad (26)$$

and

$$pmc(\Phi_R, \hat{\mathcal{M}}_{\hat{\underline{x}}}) = pmc(\Phi_R, \mathcal{M}_{\underline{x}}), \quad (27)$$

for any (quantitative) PCTL state formula Φ and reward state formula Φ_R if and only if

$$x_{z k c c'} = \sum_{\hat{k} \in [K]} \sum_{v \in \mathbb{B}^n} p_{k \hat{k} v} x_{z \hat{k} v c c'} \quad (28)$$

for all $(z, k, 3, c) \in S$ and $c' \in C$.

Proof. Let $Paths^{\mathcal{M}_{\underline{x}}}(s_0)$ and $Paths^{\hat{\mathcal{M}}_{\hat{\underline{x}}}(\hat{s}_0)}$ be the set of all $\mathcal{M}_{\underline{x}}$ paths starting at s_0 and the set of all $\hat{\mathcal{M}}_{\hat{\underline{x}}}$ paths starting at \hat{s}_0 , respectively. Equalities (26) and (27) hold iff, for any path $\pi = s_0 s_1 s_2 \dots \in Paths^{\mathcal{M}_{\underline{x}}}(s_0)$, set of associated paths $\hat{\Pi} = \{\hat{s}_0 \hat{s}_1 \hat{s}_2 \dots \in Paths^{\hat{\mathcal{M}}_{\hat{\underline{x}}}(\hat{s}_0)} \mid \forall i \geq 0. s(\hat{s}_i) = s_i\}$, and $i \geq 0$, the following property holds:

$$P(s_i, s_{i+1}) = \sum_{\hat{s}_0 \hat{s}_1 \hat{s}_2 \dots \in \hat{\Pi}} \hat{P}(\hat{s}_i, \hat{s}_{i+1}). \quad (29)$$

This is required because, according to (22) and (23), the $(i+1)$ -th state of π and of any path $\hat{\pi} \in \hat{\Pi}$ are labelled with the same atomic propositions and assigned the same state rewards, respectively; and, according to (23), the transition rewards for the transition between their i -th state and $(i+1)$ -th state are also identical. Thus, if this equality holds, the path π and path set $\hat{\Pi}$ are indistinguishable in the evaluation of PCTL state and state reward formulae; and, if the equality does not hold, a labelling function L and a PCTL state formula Φ (or state reward formula Φ_R) can be handcrafted to provide a counterexample for (26) (or for (27)).

Given the definition of \hat{P} from (21), property (29) holds trivially for any state $s_i = (z, k, t, c) \in S$ with $t=1$, and also holds for states s_i with $t=2$ because

$$\begin{aligned} \sum_{\hat{s}_0 \hat{s}_1 \hat{s}_2 \dots \in \hat{\Pi}} \hat{P}(\hat{s}_i, \hat{s}_{i+1}) &= \sum_{\hat{s}_0 \hat{s}_1 \hat{s}_2 \dots \in \hat{\Pi}} (P(s_i, s_{i+1}) \cdot p_{k \hat{k}_{i+1} v_{i+1}}) \\ &= P(s_i, s_{i+1}) \cdot \sum_{\hat{s}_0 \hat{s}_1 \hat{s}_2 \dots \in \hat{\Pi}} p_{k \hat{k}_{i+1} v_{i+1}} = P(s_i, s_{i+1}), \end{aligned}$$

where \hat{k}_{i+1} and v_{i+1} represent the DNN prediction and verification result for each state \hat{s}_{i+1} from the sum, respectively. Finally, for $t = 3$, property (29) holds if and only if the perfect-perception and DNN-perception controllers select each next controller configuration $c' \in C$ with the same probability for s_i and for all the states \hat{s}_i from $\hat{\Pi}$ taken together, i.e., if and only if (28) holds, which completes the proof. \square

Properties (26) and (27) imply that any constraint (15) is either satisfied or violated by both $\mathcal{M}_{\underline{x}}$ and $\hat{\mathcal{M}}_{\hat{x}}$ (since the two DTMCs yield the same value for the system property associated with the constraint). Likewise, $\mathcal{M}_{\underline{x}}$ and $\hat{\mathcal{M}}_{\hat{x}}$ are guaranteed to achieve the same value for the system property associated with any optimisation objective (16).

Corollary 1. *For any combination of constraints (15) and optimisation objectives (16) for which there exists a probabilistic DNN-perception controller that satisfies the constraints, there exists also a probabilistic perfect-perception controller that satisfies the same constraints and yields the same values for the PCTL properties from the optimisation objectives.*

Proof. We prove this result by showing that the application of (28) to any valid instantiation of the DNN-perception controller parameters $x_{z\hat{k}vcc'}$ produces a valid instantiation of the perfect-perception controller parameters $x_{zkc'}$. First, since $x_{z\hat{k}vcc'} \in [0,1]$ for any valid (z, \hat{k}, v, c, c') tuple, we have

$$0 = \sum_{k \in [K]} \sum_{v \in \mathbb{B}^n} (p_{kkv} \cdot 0) \leq \sum_{\hat{k} \in [K]} \sum_{v \in \mathbb{B}^n} p_{\hat{k}kv} x_{z\hat{k}vcc'} \leq \sum_{v \in \mathbb{B}^n} (p_{kkv} \cdot 1) = 1,$$

so $x_{zkc'} \in [0,1]$ for any valid tuple (z, k, c, c') . Additionally, for any valid combination of z, k and c , we have

$$\begin{aligned} \sum_{c' \in C} x_{zkc'} &= \sum_{c' \in C} \sum_{\hat{k} \in [K]} \sum_{v \in \mathbb{B}^n} p_{\hat{k}kv} x_{z\hat{k}vcc'} \\ &= \sum_{c' \in C} \left(x_{z\hat{k}vcc'} \cdot \left(\sum_{\hat{k} \in [K]} \sum_{v \in \mathbb{B}^n} p_{\hat{k}kv} \right) \right) = \sum_{c' \in C} (x_{z\hat{k}vcc'} \cdot 1) = 1, \end{aligned}$$

which completes the proof. \square

Corollary 2. *There exist an infinite number of combinations of constraints (15) and optimisation objectives (16) for which there exists a probabilistic perfect-perception controller that satisfies the constraints, and no DNN-perception controller exists that satisfies the constraints and yields the same values for the system properties from the optimisation objectives.*

Proof. We prove this result by showing that, for an infinite number of instantiations \underline{x} of the perfect-perception controller parameters $x_{zkc'}$, no valid instantiation \hat{x} of the DNN-perception controller parameters $x_{z\hat{k}vcc'}$ satisfies (28). Let $(k_0, \hat{k}_0, v_0) \in [K]^2 \times \mathbb{B}^n$ such that $p_{k_0 \hat{k}_0 v_0} \in (0,1)$. Such combinations of true class k , DNN-predicted class \hat{k} and verification results v exist, as otherwise all $p_{k\hat{k}v} \in \{0,1\}$, which would require the DNN to be perfectly accurate or to only err by always swapping class labels in the same way, and this is not possible. Consider a state $\hat{s} = (z, k, \hat{k}_0, v_0, 3, c) \in \hat{S}$, any $c' \in C$, and any of the infinite number of valid instantiations \underline{x} of the perfect-controller parameters

such that $x_{z k_0 c c'} = \alpha_{zcc'} p_{k_0 \hat{k}_0 v_0} + \sum_{(\hat{k}, v) \in [K] \times \mathbb{B}^n \setminus \{(\hat{k}_0, v_0)\}} p_{k_0 \hat{k}_0 v_0} p_{\hat{k}kv}$ with $\alpha_{zcc'} \in [0,1]$. We use (28) to calculate $x_{z \hat{k}_0 v_0 c c'}$:

$$\begin{aligned} x_{z \hat{k}_0 v_0 c c'} &= \frac{x_{z k_0 c c'} - \sum_{(\hat{k}, v) \in [K] \times \mathbb{B}^n \setminus \{(\hat{k}_0, v_0)\}} p_{k_0 \hat{k}_0 v_0} p_{\hat{k}kv} x_{z \hat{k}vcc'}}{p_{k_0 \hat{k}_0 v_0}} \\ &\geq \frac{x_{z k_0 c c'} - \sum_{(\hat{k}, v) \in [K] \times \mathbb{B}^n \setminus \{(\hat{k}_0, v_0)\}} p_{k_0 \hat{k}_0 v_0} p_{\hat{k}kv}}{p_{k_0 \hat{k}_0 v_0}} \\ &= \frac{\alpha_{zcc'} p_{k_0 \hat{k}_0 v_0}}{p_{k_0 \hat{k}_0 v_0}} = \alpha_{zcc'}. \end{aligned}$$

Accordingly, the outgoing transition probabilities from the considered state \hat{s} add up to

$$\sum_{c' \in C} x_{z \hat{k}_0 v_0 c c'} \geq \sum_{c' \in C} \alpha_{zcc'}. \quad (30)$$

As the right-hand side of this inequality can take any value in the interval $[0, \#C]$, and the only valid value for $\sum_{c' \in C} x_{z \hat{k}_0 v_0 c c'}$ is 1, we identified an infinite number of instantiations \underline{x} for which a valid instantiation \hat{x} cannot be built. \square

Corollary 2 shows that the decision-making capabilities of infinitely many perfect-perception controllers cannot be replicated by DNN-perception controllers. While this does not indicate how many of these practically unachievable controllers satisfy constraints (15) and Pareto-optimalise objectives (16), the proof of the corollary provides a hint about this by showing in (30) that DNN-perception controllers do not exist for large $\alpha_{zcc'}$ values, i.e., for scenarios when the perfect-perception controller decides to use a specific configuration c with high probability. Intuitively, these scenarios are highly relevant, i.e., many perfect-perception controllers with no equivalent DNN-perception controllers are likely to be Pareto-optimal. For instance, the perfect-perception controller used for the mobile robot application from the next section decides that the robot should mostly or even always wait when a collision with another mobile agent would otherwise occur. This line of reasoning also implies that deterministic perfect-perception controllers are likely to not have equivalent (probabilistic or deterministic) DNN-perception controllers.

Stage 3: Controller synthesis. The controller synthesis problem for the DNN-perception system involves finding instantiations \hat{x} of the DNN-perception controller parameters for which the pDTMC $\hat{\mathcal{M}}$ from (17) satisfies the constraints (15) and is Pareto optimal with respect to the optimisation objectives (16). Solving the general version of this problem precisely is unfeasible. However, metaheuristics such as multi-objective genetic algorithms for probabilistic model synthesis^{19,20} can be used to generate close approximations of the Pareto-optimal controller set. Alternatively, exhaustive search can be employed to synthesise the actual Pareto-optimal controller set for systems with deterministic controllers and small numbers of controller parameters, or—by discretising the search space—an approximate Pareto-optimal controller set for systems with probabilistic controllers. We demonstrate the synthesis of DEEPDECS controllers through the use of both metaheuristics and exhaustive search in the next section.

2 DEEPDECS Applications

Mobile-robot collision limitation. Recent research proposes the use of DNN perception in the collision avoidance systems of unmanned aircraft,^{21,22} autonomous marine vehicles²³ and autonomous mobile robots.²⁴ We used DEEPDECS to develop a mobile robot collision-limitation controller inspired by these applications. As shown in Figure 3a, we considered a service robot tasked with travelling autonomously from location A to location B, e.g., for the purpose of carrying goods in a warehouse or hospital. Within this environment, the robot may encounter and potentially collide with another moving autonomous agent. We assume that these collisions are not catastrophic, but that they incur damage to the robot and slow it down. As such, the robot uses DNN perception to assess the risk of collision at each intermediate waypoint I, and decides whether to proceed to the next waypoint or to wait for a while at waypoint I based on the DNN output.

The logic underpinning the operation of the robot at any intermediate waypoint I is modelled by the perfect-perception pDTMC in Figure 3b. As shown by the **MobileRobot** pDTMC module, when reaching waypoint I the robot first uses its sensors (lidar, cameras, etc.) to **look** for the “collider” (state $z = 0$). If the collider is present in the vicinity of the robot (which happens with probability p_{collider} , known from previous executions of the task), the robot performs a **check** action (state $z = 1$). As defined in the module **Collider**, this leads to the execution of a **monitor** action to predict whether travelling to the next waypoint would place the robot on collision course with the other agent (which happens with probability p_{occ} , also known from historical data) or not. Each **monitor** action activates the controller, whose behaviour is specified by the **PerfectPerceptionController** module. A probabilistic controller with two parameters is used: the controller decides that the robot should wait with probability x_1 when no collision is predicted ($k = 1$) and with probability x_2 if a collision is predicted ($k = 2$). Depending on this decision, the robot will either **retry** after a short wait or **proceed** and **travel** to the next waypoint, reaching the **end** of the decision-making process. Finally, when the collider is absent (with probability $1 - p_{\text{collider}}$ in the first line from the **MobileRobot** module), the robot can **travel** without going through these intermediate actions.

We used data from a simulator of the scenario in Figure 3a to train a collision-prediction DNN. We then applied DEEPDECS (Figure 1) to this DNN, a test dataset collected using the same simulator, the perfect-perception pDTMC model from Figure 3b, and a set of PCTL-encoded requirements demanding controllers that can (a) guarantee a collision-free journey with probability of at least 0.75:

$$C_1: \quad \mathcal{P}_{\geq 0.75}[\neg \text{collision} \wedge \text{done}] \quad (31)$$

and (b) achieve an optimal trade-off between maximising this probability and minimising the travel time:

$$\begin{aligned} O_1: & \text{ maximise } \mathcal{P}_{=?}[\neg \text{collision} \wedge \text{done}] \\ O_2: & \text{ minimise } \mathcal{R}_{=?}^{\text{time}}[\text{F done}] \end{aligned} \quad (32)$$

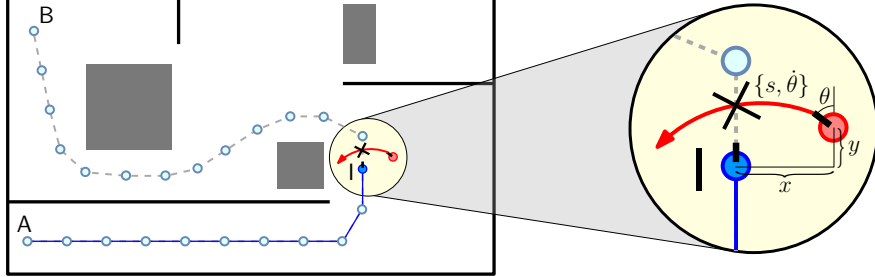
We applied DEEPDECS to these inputs four times, using different combinations of DNN verification methods in the

DNN uncertainty quantification stage: (i) no DNN verification method; (ii) only verif_1 from (4); (iii) only verif_2 from (3); and (iv) both verif_1 and verif_2 . Figure 3c shows DNN-perception pDTMC model produced by the model augmentation DEEPDECS stage for combination (ii), and Figure 4 presents the results from the other DEEPDECS stages and from the testing of the synthesised controllers for all combinations. Figure 4a presents the probability of the DNN making a correct prediction across the four setups after training. The DNN achieved high accuracy, and as verification methods are introduced it is observed that the “verified” predictions have a higher probability of being correct.

The controller design space was explored via discretising the parameter space, with each of the parameters $x_{1\text{false}}$, $x_{1\text{true}}$, $x_{2\text{false}}$ and $x_{2\text{true}}$ varied between 0 and 1 with a step size of 0.1, and every $(x_{1\text{false}}, x_{1\text{true}}, x_{2\text{false}}, x_{2\text{true}})$ combination obtained in this way was analysed. The setup with perfect perception (Figure 3b) was analysed similarly for evaluation purposes. Pareto fronts were generated from the modelled controller parameter combinations, see Figure 4b, clearly showing an intuitive balance of collision probability and time to complete journey; to achieve a faster time the less likely it will be a safe journey. The optimal results, expectedly, are achieved with a perfect perception, and the front achieved when no verification DNN method is used is always outperformed by the perfect perception front, other than at two extreme points. When verification methods are introduced, the Pareto fronts improve and get closer to the perfect DNN Pareto front. There are three instances where the Pareto fronts achieve the same result; first when the parameters are all set to 0 (travel regardless of prediction), 0.5 (always flip a balanced coin regardless of prediction), or 1 (always wait when there is a collider present).

We used two established Pareto front indicators to analyse the quality of the Pareto fronts: the Inverse Generational Distance (IGD)²⁵ and the Hypervolume (HV).²⁶ IGD uses a reference frame and calculates, for each point on the reference frame, the distance to the closest point on the Pareto front, with an average then extracted. HV also uses a reference frame to generate a nadir point which is then used with the Pareto front to determine how much of a region is covered by said Pareto front. Smaller IGD and higher HV values indicate a better Pareto front. The reference frame used for both IGD and HV was the Pareto front generated from the perfect perception setup, since this is the ideal Pareto front that a 100% accurate DNN would achieve. From these indicators it is observed that the setups using verification methods produce higher quality Pareto fronts than the no verification DNN method, see Figure 4c. Both IGD and HV also indicate that using both verification methods led to a better Pareto front than just utilising one verification method.

The Pareto fronts generated from the models were validated by integrating the synthesised controllers with the original mobile-robot simulation. With each synthesised controller, the simulator conducted a number of journeys for the robot with the same probabilities of collider presence and resultant collision if the robot was to travel, with an average time and probability of robot collision extracted. As the number of waypoints across these journeys increases, the difference



(a) A mobile robot (darker blue) travelling between locations A and B may collide with another mobile agent (red) when moving from its current waypoint I to the next waypoint. A two-class DNN predicts whether the robot is on collision course based on the relative horizontal distance x and vertical distance y between the robot and the collider, and the speed s , angle θ and angular velocity $\dot{\theta}$ of the collider.

```
dtmc
const double Pcollider = 0.8;
module MobileRobot // ManagedComponents
  z : [0..4] init 0; // 0:check collider, 1:collider detected,
                      // 2:check wait, 3:no collider, 4:done
  [look] t=1 ∧ z=0 → Pcollider:(z'=1) + (1-Pcollider):(z'=3);
  [check] t=1 ∧ z=1 → 1:(z'=2);
  [retry] t=1 ∧ z=2 ∧ wait → 1:(z'=0);
  [proceed] t=1 ∧ z=2 ∧ ¬wait → 1:(z'=3);
  [travel] t=1 ∧ z=3 → 1:(z'=4);
  [end] t=1 ∧ z=4 → 1:(z'=4);
endmodule

const double Pocc = 0.25;
module Collider // Environment
  k : [1..2] init 1; // 1:not on collision course (occ), 2:occ
  [monitor] t=2 → (1-Pocc):(k'=1) + Pocc:(k'=2);
endmodule

const double x1; // prob. of waiting when occ
const double x2; // prob. of waiting when not occ

module PerfectPerceptionController
  wait : bool init false;
  [reaction] t=3 ∧ k=1 → x1:(wait'=true) + (1-x1):(wait'=false);
  [reaction] t=3 ∧ k=2 → x2:(wait'=true) + (1-x2):(wait'=false);
endmodule

module Turn
  t : [1..3] init 1;
  [check] true → 1:(t'=2);
  [monitor] true → 1:(t'=3);
  [decide] true → 1:(t'=1);
endmodule

rewards "time"
  [travel] true : 9.95;
  [proceed] k=2 : 2.57;
  [retry] true : 5;
endrewards

label "collision" = z=3 & k=2;
label "done" = z=4;
```

(b) Perfect-perception pDTMC model of the mobile robot journey between two successive waypoints. The model states are tuples $(z, k, t, \text{wait}) \in \{0, 1, \dots, 4\} \times [2] \times [3] \times \mathbb{B}$ with the semantics from (11). The reward structure models the **time** taken by each robot actions: 9.95 time units to **travel** between adjacent waypoints (without collision), 2.57 additional time units when the robot decides to **go** despite being on collision course, and five time units when the robot decides to **retry** after a short wait; the other robot actions are assumed to take negligible time. Two atomic propositions are used by the labelling function at the end of the model: **collision**, for states in which the robot travels despite being on collision course, and **done**, for states that mark the end of the journey.

```
dtmc
const double Pcollider = 0.8;
module MobileRobot // ManagedComponents
  z : [0..4] init 0;
  [look] t=1 ∧ z=0 → Pcollider:(z'=1) + (1-Pcollider):(z'=3);
  [check] t=1 ∧ z=1 → 1:(z'=2);
  [retry] t=1 ∧ z=2 ∧ wait → 1:(z'=0);
  [proceed] t=1 ∧ z=2 ∧ ¬wait → 1:(z'=3);
  [travel] t=1 ∧ z=3 → 1:(z'=4);
  [end] t=1 ∧ z=4 → 1:(z'=4);
endmodule

const double Pocc = 0.25;
const double P11false = eq. (7)
...
const double P22true = eq. (7)

module ColliderWithDNNPerception // EnvironmentWithDNNPerception
  k : [1..2] init 1; // 1:not occ, 2:occ
  k̂ : [1..2] init 1; // DNN predicts 1:not occ, 2:occ
  v1 : bool init false;
  [monitor] t=2 → (1-Pocc)·P11false:(k'=1) & (k̂'=1) & (v1'=false)
            + (1-Pocc)·P11true:(k'=1) & (k̂'=1) & (v1'=true)
            + (1-Pocc)·P12false:(k'=1) & (k̂'=2) & (v1'=false)
            + (1-Pocc)·P12true:(k'=1) & (k̂'=2) & (v1'=true)
            + Pocc·P21false:(k'=2) & (k̂'=1) & (v1'=false)
            + Pocc·P21true:(k'=2) & (k̂'=1) & (v1'=true)
            + Pocc·P22false:(k'=2) & (k̂'=2) & (v1'=false)
            + Pocc·P22true:(k'=2) & (k̂'=2) & (v1'=true);
endmodule

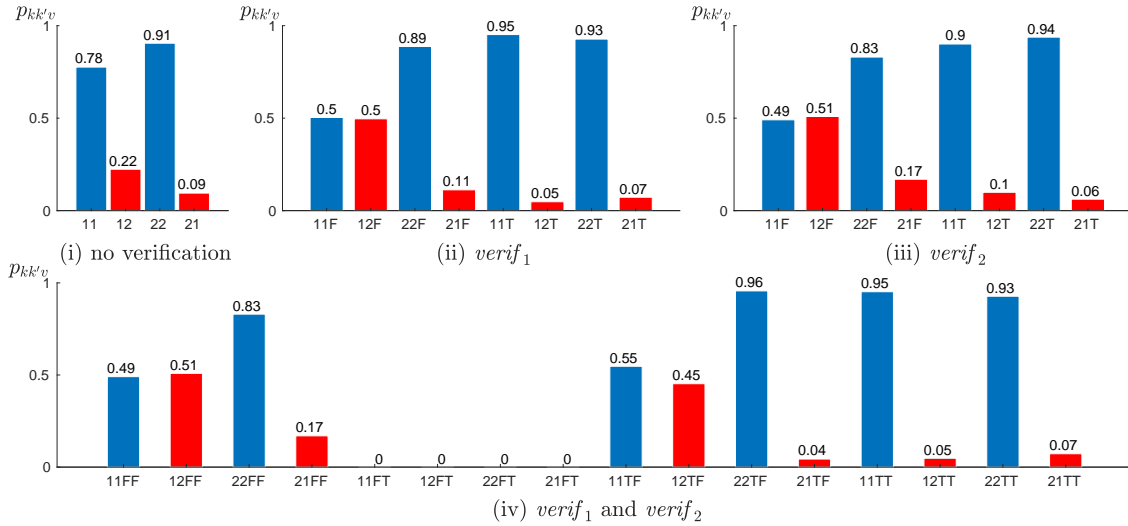
const double x1false; // DNN predicts not occ and v1 returns false
const double x1true; // DNN predicts not occ and v1 returns true
const double x2false; // DNN predicts occ and v1 returns false
const double x2true; // DNN predicts occ and v1 returns true

module DNNPerceptionController
  wait : bool init false;
  [decide] t=3 ∧ k̂=1 ∧ ¬v1 → x1false:(wait'=true) + (1-x1false):(wait'=false);
  [decide] t=3 ∧ k̂=1 ∧ v1 → x1true:(wait'=true) + (1-x1true):(wait'=false);
  [decide] t=3 ∧ k̂=2 ∧ ¬v1 → x2false:(wait'=true) + (1-x2false):(wait'=false);
  [decide] t=3 ∧ k̂=2 ∧ v1 → x2true:(wait'=true) + (1-x2true):(wait'=false);
endmodule

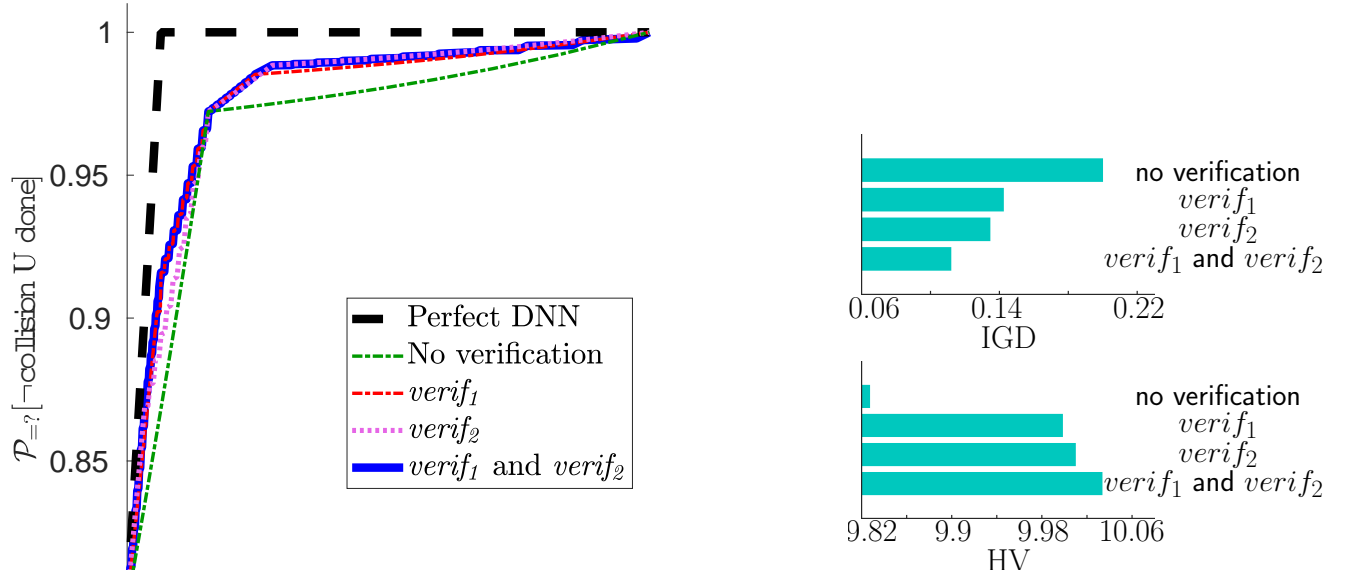
module Turn
  t : [1..3] init 1;
  [check] true → 1:(t'=2);
  [monitor] true → 1:(t'=3);
  [decide] true → 1:(t'=1);
endmodule
```

(c) DNN-perception pDTMC model of the mobile robot journey between two successive waypoints. The probabilities $p_{kk'v_1}$ from the **ColliderWithDNNPerception** module quantify the DNN accuracy for “verified” inputs ($v_1 = \text{true}$) and “unverified” inputs ($v_1 = \text{false}$), and are used to model the class \hat{k} predicted by the DNN when the true class is k . The decisions of the four-parameter probabilistic controller depend on the DNN prediction \hat{k} and the online verification result v_1 .

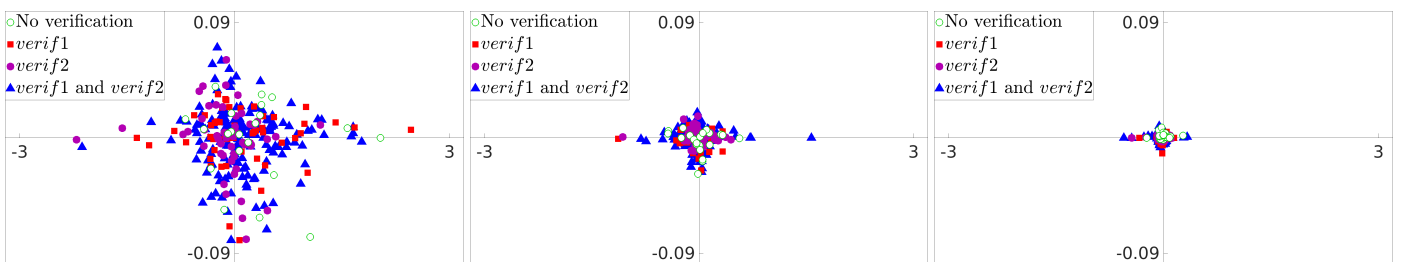
Figure 3: Collision limitation for a mobile robot tasked with traversing a known environment through the use of waypoints



(a) Probability that a class- k DNN input is (mis)classified as class k' and satisfies $verif_i = (v_1, v_2, \dots, v_n) \in \mathbb{B}^n$



(b) Pareto front associated with the set of Pareto-optimal DEEPDECS controllers



(d) Difference between the model-based and simulation-based probability of collision-free travel and travel time for the Pareto-optimal DEEPDECS controllers from Figure 4b for 100 waypoints (left), 1000 waypoints (middle) and 10000 waypoints (right).

Figure 4: DEEPDECS controller synthesis and testing results for the mobile robot collision limitation

between the simulator and the model decreases, see Figure 4d, thus validating the models and controllers used.

Driver-attentiveness management. The recent adoption of the first United Nations regulation on vehicles with Level 3 automation²⁷ has paved the way for the safe introduction of shared-control passenger cars with Automated Lane Keeping Systems (ALKS). In certain traffic environments detailed in the regulation—and for as long as the driver is attentive—these cars will be able to drive entirely autonomously. However, ALKS can issue *transition demands* requesting the driver to take over the driving task when the car approaches traffic conditions outside its ODD. Transition demands will be issued timely, enabling an attentive driver to resume manual driving safely. If the driver is unresponsive or becomes inattentive and ALKS-issued alerts meant to restore driver attentiveness are ineffective, a *minimum-risk manoeuvre* (e.g., bringing the car to a standstill) will be performed.

We applied DEEPDECS to design a proof-of-concept driver attentiveness management system for ALKS-enabled cars. Developed as part of our SafeSCAD project^f, this system uses (Figure 5a): (i) specialised sensors to monitor key car parameters (velocity, lane position, etc.) and driver’s biometrics (eye movement, heart rate, etc.), (ii) a DNN to predict the driver’s response to a transition demand, and (iii) a software controller to issue visual/acoustic/haptic alerts when the driver is inattentive.

We used an existing DNN trained and validated with driver data from a SafeSCAD user study carried out within a driving simulator.²⁸ The test dataset used for our DNN uncertainty quantification came from the same study, and the perfect-perception pDTMC model provided to DEEPDECS (shown in Figure 5b) is a significantly revised version of a model we proposed in preliminary SafeSCAD work.²⁹ Finally, the controller requirements comprise two constraints that limit the maximum expected risk and driver nuisance accrued over a 45-minute driving trip, and two optimisation objectives requiring that the same two measures are minimised:

$$\begin{aligned} C_1: & \mathcal{R}_{\leq 100}^{\text{risk}}[C^{\leq 2000}] \\ C_2: & \mathcal{R}_{\leq 6 \times 10^3}^{\text{nuisance}}[C^{\leq 2000}] \\ O_1: & \text{minimise } \mathcal{R}_{=?}^{\text{risk}}[C^{\leq 2000}] \\ O_2: & \text{minimise } \mathcal{R}_{=?}^{\text{nuisance}}[C^{\leq 2000}] \end{aligned} \quad (33)$$

where each occurrence of the PCTL reward operator \mathcal{R} is annotated with the name of the reward structure from Figure 5b it refers to (i.e., ‘risk’ or ‘nuisance’). The 2000 time-steps from the PCTL cumulative reward properties correspond to the 45 minutes of the journey: verifying the driver state every 4s requires 667 verifications over 2667s, and each verification is modelled by three pDTMC time-steps, one for the **monitoring** of the driver state, one for the controller to **decide** the appropriate alerts for the observed state, and one for the decided alerts to be issued in order to **warn** the driver.

The DNN verification methods verif_1 and verif_2 from (3) and (4) were used in all possible combinations (i.e., alone, together, and neither) in the DEEPDECS DNN uncertainty

quantification stage. Figure 6a shows the DNN-perception pDTMC obtained in the model augmentation stage using verification results produced when verif_1 was used alone, and Figures 6b and 6c compare the controller Pareto fronts obtained for all these combinations to the Pareto front associated with the perfect-perception model from Figure 5b.

The search space in this case study (8¹² controller parameter combinations when both DNN verification methods are used) is significantly larger than for the discretised robot collision avoidance scenario. As such, an exhaustive search to determine the Pareto-optimal controllers is infeasible. Therefore EvoChecker,²⁰ which adopts multiobjective genetic algorithms, was employed to generate close approximations of the Pareto-optimal controllers. The Pareto fronts, see Figure 6b, convey a similar relationship to that displayed by the Pareto fronts in the robot collision avoidance case; the inclusion of verification methods achieves Pareto-optimal controllers closer to the perfect-perception Pareto fronts. Furthermore, the knee point of the verif_1 and verif_1 and verif_2 fronts are closest to the knee point of the perfect DNN front. These two fronts share a similar frontier in general. This is reflected further in the quantitative analysis, Figure 6c, with the IGD values of these fronts being the smallest out of the four setups.

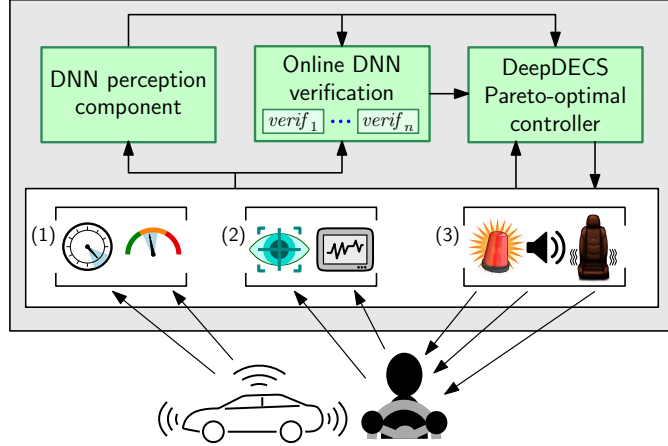
The HV indicator also supports inclusion of verification methods, as it strongly shows the no verification setup performs the worse. The two best setups were, again, verif_1 on its own and the verif_1 and verif_2 setup, with HV values of 8.91×10^5 and 8.89×10^5 respectively. This is still quite a large gap between the two fronts, though this is not surprising. The verif_1 Pareto front has the extremes significantly further apart, thus resulting in a significantly higher HV value. It is perhaps best to note that the two absolute extremes can be achieved in all setups; for minimised risk, perform the most cautious action of issuing all alerts regardless of driver’s attention, and vice versa for minimising nuisance. The state space for a controller integrated with two verification methods is twice the size of using only one, which therefore requires a significantly larger evaluation time to properly search and find the Pareto-optimal controller. We expect that if the population size and evaluation are of substantial size, the two extremes would be found (in all setups) and the HV would in turn favour the verif_1 and verif_2 setup.

Another interesting outcome is that while the same verification methods were applied to both studies, the different scenarios dictated which method was more valuable; verif_2 in the robot collision avoidance study and verif_1 in the SafeSCAD scenario. This is indicative of the appropriateness of creating the confusion matrices and models with respect to the specific verification methods outcomes rather than using a collective count of verification methods satisfied.

3 Discussion

To operate safely and effectively, autonomous systems need to perceive, and respond to, changes in their environment. Increasingly, this perception involves some form of machine learning—often a deep-learning component that maps sensor data to predefined classes of environmental states or events. Autonomous system controllers, typically implemented as tra-

^fSafety of Shared Control in Autonomous Driving (cutt.ly/Safe-SCAD)



(a) SafeSCAD driver-attentiveness management system. Data from car sensors (1) and driver biometric sensors (2) are supplied to a DNN perception component that classifies the driver state as attentive, semi-attentive or inattentive. The DEEPDECS controller decides when optical, acoustic and/or haptic alerts (3) should be used to increase the driver's attentiveness.

```

1  dtmc
2
3  module Alerts // ManagedComponents
4    z : [0..7] init 0;
5
6    [warn] t=1 → 1:(z'=c);
7  endmodule
8
9  // probabilities  $pd_{kk'c}$  that driver attentiveness changes from level  $k \in \{1, 2, 3\}$  to level  $k' \in \{1, 2, 3\}$  given alerts  $z \in \{0, 1, \dots, 7\}$ 
10 const double pd110 = 0.99775;
...
81 const double pd337 = 0.809;
82
83 module Driver // Environment
84   k : [1..3] init 1; // driver status: attentive ( $k = 1$ ); semi-attentive ( $k = 2$ ); or inattentive ( $k = 3$ )
85
86   // driver attentiveness changes from level  $k \in \{1, 2, 3\}$  to level  $k' \in \{1, 2, 3\}$  given alerts  $z \in \{0, 1, \dots, 7\}$ 
87   [monitor] t=2 ∧ k=1 ∧ z=0 → pd110:(k'=1) + pd120:(k'=2) + pd130:(k'=3);
...
110  [monitor] t=2 ∧ k=3 ∧ z=7 → pd317:(k'=1) + pd327:(k'=2) + pd337:(k'=3);
111 endmodule
112
113 const int x1; // alerts to be issued when driver is found attentive ( $k = 1$ )
114 const int x2; // alerts to be issued when driver is found semi-attentive ( $k = 2$ )
115 const int x3; // alerts to be issued when driver is found inattentive ( $k = 3$ )
116
117 module PerfectPerceptionController
118   c : [0..7] init 0;
119
120   [decide] t=3 ∧ k=1 → 1:(c'=x1);
121   [decide] t=3 ∧ k=2 → 1:(c'=x2);
122   [decide] t=3 ∧ k=3 → 1:(c'=x3);
123 endmodule
124
125 module Turn
126   t : [1..3] init 1;
127
128   [warn] true → 1:(t'=2);
129   [monitor] true → 1:(t'=3);
130   [decide] true → 1:(t'=1);
131 endmodule
132
133 // risk when driver is not attentive
134 rewards "risk"
135   [monitor] k=1 : 0; // no risk
136   [monitor] k=2 : 1; // low risk
137   [monitor] k=3 : 4; // high risk
138 endrewards
139
140 // driver nuisance caused by alerts
141 rewards "nuisance"
142   [monitor] z=1 : (k=1)?6:2;
143   [monitor] z=2 : (k=1)?3:1;
144   [monitor] z=3 : (k=1)?8:3;
145   [monitor] z=4 : (k=1)?10:3;
146   [monitor] z=5 : (k=1)?16:5;
147   [monitor] z=6 : (k=1)?11:4;
148   [monitor] z=7 : (k=1)?20:6;
149 endrewards

```

(b) Perfect-perception pDTMC model of the SafeSCAD system. The model states are tuples $(z, k, t, c) \in [7] \times [3]^2 \times \{0, 1, \dots, 7\}$ with the semantics from (11). The **Alerts** module is responsible for **warning** the driver by “implementing” the controller-decided alerts c . The **Driver** module models the driver attentiveness level k , which is **monitored** every 4s; the probabilities of transition between attentiveness levels depend on the combination of alerts z in place. The control parameters $x_1, x_2, x_3 \in \{0, 1, \dots, 7\}$ are binary encodings of the alerts to be activated for each of the three driver attentiveness levels, e.g., $x_3 = 5 = 101_{(2)}$ corresponds to a deterministic-controller decision to have the optical alert active, the acoustic alert inactive, and the haptic alert active when the driver is inattentive. The reward structures from lines 134–138 and 141–149 quantify the risk and driver nuisance associated with the different driver attentiveness levels and alert combinations, respectively. The expressions ‘ $(k=1)?value_1:value_2$ ’ from lines 142–148 evaluate to the larger $value_1$ if the driver is attentive (i.e., $k=1$), and $value_2$ otherwise.

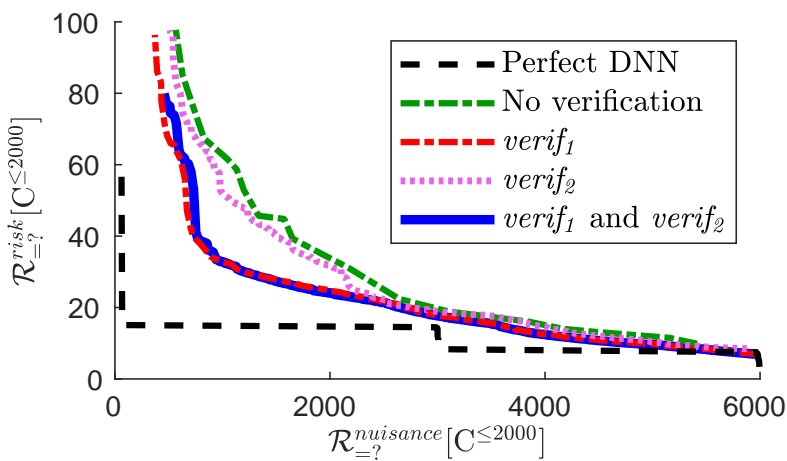
Figure 5: Driver-attentiveness management for shared-control autonomous driving

```

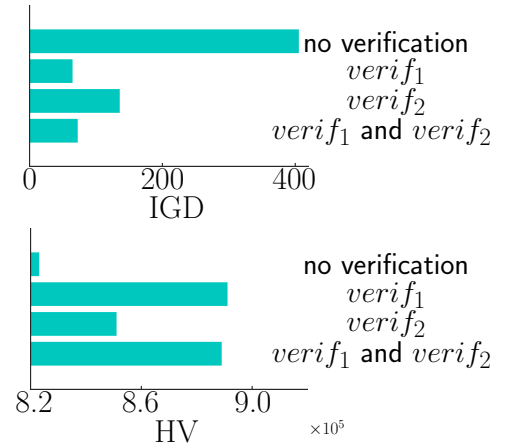
1  dtmc
2
3  module Alerts // ManagedComponents
4    z : [0..7] init 0;
5
6    [warn] t=1 → 1:(z'=c);
7  endmodule
8
9  // probabilities  $pd_{kk'c}$  that driver attentiveness changes from level  $k \in \{1, 2, 3\}$  to level  $k' \in \{1, 2, 3\}$  given alerts  $z \in \{0, 1, \dots, 7\}$ 
10 const double pd110 = 0.99775;
...
11 const double pd337 = 0.809;
12
13 // probabilities  $p_{kk'v_1}$  that DNN (mis)classifies the driver state  $k$  as  $\hat{k}$  when the online verification result is  $v_1$ 
14 const double p11false = eq. (7)
...
15 const double p33true = eq. (7)
16
17 module DriverWithDNNPerception // EnvironmentWithDNNPerception
18   k : [1..3] init 1; // driver status: attentive ( $k = 1$ ); semi-attentive ( $k = 2$ ); or inattentive ( $k = 3$ )
19   k : [1..3] init 1; // DNN-predicted driver status: attentive ( $\hat{k} = 1$ ); semi-attentive ( $\hat{k} = 2$ ); or inattentive ( $\hat{k} = 3$ )
20   v1 : bool init false;
21
22   // driver attentiveness changes from level  $k$  to true level  $k'$  and DNN-predicted level  $\hat{k}'$  given alerts  $z$ 
23   [monitor] t=2 ∧ k=1 ∧ z=0 → pd110·p11false:(k'=1) & (k'=1) & (v1'=false) + pd110·p11true:(k'=1) & (k'=1) & (v1'=true) +
24     pd110·p12false:(k'=1) & (k'=2) & (v1'=false) + pd110·p12true:(k'=1) & (k'=2) & (v1'=true) +
25     pd110·p13false:(k'=1) & (k'=3) & (v1'=false) + pd110·p13true:(k'=1) & (k'=3) & (v1'=true) +
26     pd120·p21false:(k'=2) & (k'=1) & (v1'=false) + pd120·p21true:(k'=2) & (k'=1) & (v1'=true) +
27     pd120·p22false:(k'=2) & (k'=2) & (v1'=false) + pd120·p22true:(k'=2) & (k'=2) & (v1'=true) +
28     pd120·p23false:(k'=2) & (k'=3) & (v1'=false) + pd120·p23true:(k'=2) & (k'=3) & (v1'=true) +
29     pd130·p31false:(k'=3) & (k'=1) & (v1'=false) + pd130·p31true:(k'=3) & (k'=1) & (v1'=true) +
30     pd130·p32false:(k'=3) & (k'=2) & (v1'=false) + pd130·p32true:(k'=3) & (k'=2) & (v1'=true) +
31     pd130·p33false:(k'=3) & (k'=3) & (v1'=false) + pd130·p33true:(k'=3) & (k'=3) & (v1'=true);
32
33 endmodule
34
35 const int x1false; // alerts to be issued when driver is classified attentive ( $\hat{k} = 1$ ) and verification result is false
...
36 const int x3true; // alerts to be issued when driver is classified inattentive ( $\hat{k} = 3$ ) and verification result is true
37
38 module DNNPerceptionController
39   c : [0..7] init 0;
40
41   [decide] t=3 ∧ k=1 ∧ ¬v1 → 1:(c'=x1false);
...
42   [decide] t=3 ∧ k=3 ∧ v1 → 1:(c'=x3true);
43 endmodule
44
45 module Turn
46
47 endmodule
48
49 endmodule

```

(a) DNN-perception pDTMC model of the SafeSCAD driver-attentiveness management system for the scenario when a single DNN verification method is used to distinguish between “verified” ($v_1 = \text{true}$) and “unverified” ($v_1 = \text{false}$) DNN predictions of the driver’s attentiveness level. Lines 103–111 show how all combinations of true (k') and DNN-predicted (\hat{k}') driver attentiveness levels can be reached from the attentive driver state ($k = 1$) when no alerts are used ($c = 0$). The six-parameter deterministic controller decides a combination of alerts c for each pair of DNN-predicted driver attentiveness level \hat{k} and online DNN verification result v_1 (lines 339–344). The **Switch** module and the two reward structures from the pDTMC in Figure 5b are omitted for brevity.



(b) Pareto front associated with the set of Pareto-optimal SafeSCAD controllers



(c) Evaluation of Pareto front quality using the established IGD and HV metrics.

Figure 6: DEEPDECS controller synthesis model and results for the driver-attentiveness management system

ditional-software components, can then consider these states and events in their decision making. However, deep-learning components can never be 100% accurate. This limitation poses a major challenge to established controller development methods. The DEEPDECS method introduced in our paper addresses this challenge through several key contributions.

First, we devised a new approach to quantifying aleatory DNN uncertainty within the ODD of an autonomous system. Using a suite of n DNN verification techniques, this approach identifies 2^n categories of DNN outputs, each of which is associated with a different trustworthiness level. The uncertainty of each category of DNN outputs is then separately quantified using a unique combination of development-time and online DNN verification. This enables the controllers of autonomous systems to consider each category of DNN outputs differently. In particular, these controllers can react confidently to highly trustworthy DNN outputs, and conservatively to DNN outputs associated with low trustworthiness levels. Importantly, we showed experimentally that the vast majority of DNN outputs fell into the former category for the DNN-perception components of two autonomous systems from different application domains. Our approach to quantifying DNN uncertainty opens up the opportunity to leverage the broad range of recently devised DNN verification techniques^{8–10, 12, 30–32} that certify DNN properties like local robustness and confidence.

Second, we developed a theoretical foundation for the integration of DNN-perception uncertainty into discrete-time stochastic models describing the behaviour of autonomous systems. The new theory enables the formal analysis of safety, dependability, performance and other key properties of autonomous systems with necessarily imperfect deep-learning perception components. Furthermore, it supports the formal modelling of autonomous systems that use any combination of online DNN verification techniques to quantify their environment perception uncertainty.

Third, we showed how the DEEPDECS parametric DTMC models of DNN-perception autonomous systems can be used to synthesise both deterministic and probabilistic discrete-event controllers for these systems. Given n_1 constraints and n_2 optimisation objectives that formalise in probabilistic temporal logic the safety, dependability and performance requirements of an autonomous system, this synthesis yields controllers guaranteed to satisfy the n_1 constraints and that are Pareto-optimal with respect to the n_2 optimisation objectives. Importantly, we showed how using larger numbers of DNN verification techniques produces better sets of Pareto-optimal controllers.

Finally, we demonstrated the applicability of DEEPDECS within two case studies from different application domains. For the first case study, we synthesised probabilistic collision-limitation controllers for a mobile robot travelling in an environment where another moving autonomous agent may also be present. To obtain these controllers, we discretised the controller parameter space, and then performed an exhaustive search over all possible combinations of discretised parameter values. For the second case study, we used multi-objective genetic algorithms to synthesise deterministic controllers for a driver-attentiveness management system.

While our paper focuses on controller synthesis for

autonomous systems with DNN perception components, DEEPDECS is not prescriptive about the type of machine learning (ML) components that introduce uncertainty into autonomous systems. We therefore envisage that DEEPDECS is equally applicable to additional such systems, as long as analogous ML verification methods exist to enable the quantification of the aleatory uncertainty introduced by their ML components. Examples of other ML techniques that utilise confidence measures to quantify the uncertainty of their predictions include support vector machines and Gaussian processes.

While the design of autonomous systems that use DNN classifiers for perception in combination with discrete-event controllers for decision-making has been studied,^{33–35} synthesizing safe and optimal discrete-event controllers that account for the uncertainty in the DNN outcomes is a novel contribution of this work. Additionally, our DNN uncertainty quantification mechanism, which uses the outcomes of off-the-shelf DNN verifiers in a black-box manner, is also new.

Related work includes the approach of Jha et al.³³ that synthesise correct-by-construction controllers for autonomous systems with noisy sensors, i.e., with perception uncertainty. Unlike our approach, they only consider systems using linear models (i.e., not DNNs) for perception where the uncertainty quantities are already known. Moreover, while we formulate the control problem as a PDTMC, Jha et al. consider the simpler setting of deterministic linear systems. Michelmore et al.³⁴ analyze the safety of autonomous driving control systems that use DNNs in an end-to-end manner for both perception and control, i.e., the DNN consumes sensor readings and outputs control actions. They use Bayesian methods for calculating the uncertainty in the control actions predicted by the DNN, and in case the DNN uncertainty is higher than pre-determined thresholds, the system defaults to executing fail-safe actions. In contrast, we synthesise controllers that can use the quantified uncertainty of DNN perception in order to select optimal yet safe actions. Cleaveland et al.³⁵ study verification of autonomous systems with machine learning-based perception. They are interested in situations where the controller has already been constructed and the uncertainty in the perception outcomes is known, so the only goal is to verify if the autonomous system satisfies a required probabilistic specification of safety.

There is a large body of work on quantifying the uncertainty in DNN classifiers. One major approach is to consider K -class DNN classifiers as functions that map an input $x \in \mathbb{R}^d$ to a discrete probability distribution over K classes. The probability associated with a class is then interpreted as the probability that the class is the *true label* of x . For these probability estimates to be useful for downstream decision-making, it is essential that the DNN is well-calibrated, i.e., the predicted probabilities are close to the true probabilities. Formally, a DNN f is perfectly calibrated if the following holds,

$$\forall p \in [0,1]. \quad \mathbb{P}_{x \sim D} [y = f^*(x) \mid \hat{p} = p] = p, \quad (34)$$

where $y = \text{argmax}_{i \in [K]} \{f(x)_i\}$, i.e., y is the predicted label, and $\hat{p} = f(x)_y$, i.e., \hat{p} is the estimated probability associated with the predicted label. It has been shown that modern DNNs are not well-calibrated.¹² Even with carefully designed interventions to ensure well-calibration, there is no guarantee that the proba-

Table 1: Robot collision avoidance parameters

Parameter	Value
α	0.5
x_{goal}	0
y_{goal}	10
ϵ	0.05
x_{lim}	10
y_{lim}	10
s_{lim}	2 units/s
$\dot{\theta}_{lim}$	$\frac{\pi}{4}$ rads/s

bility estimates are close to the true values. Another approach to quantifying the uncertainty of DNN prediction is to use Bayesian techniques. In particular, Bayesian Neural Networks (BNNs) have been proposed as a Bayesian extension of DNNs. As opposed to DNNs where the weights θ associated with a DNN are fixed, BNNs consider a distribution over the weights, and the BNN prediction is the expected outcome with respect to the weights distribution. While a BNN can produce an estimate of the prediction uncertainty, even these estimates are not necessarily well-calibrated due to the possibility of model mis-specification.³⁶ Alternately, techniques based on conformal prediction^{37,38} can be used to construct prediction sets,³⁹ i.e., a set of predicted values instead of a single predicted value for a given input, such that the true label is guaranteed to be in the prediction set with a user-controllable probability.

4 Methods

Dataset collection. We obtained the dataset for the collision avoidance study using the 2D particle simulator *Box2D* (<https://box2d.org/>). The robot and collider were circular particles with radius of 0.5 units. The robot was initialised at the origin with a heading of $\frac{\pi}{2}$ radians, however the robot only considers the local coordinate frame with itself as the reference, i.e. the initial heading is also 0 radians. The robot would travel in a straight line to the goal destination at coordinate (0,10) with a speed of 1 unit per second. The robot is considered to have successfully completed the journey if the robot is within the goal area which is defined as

$$(\hat{x}, \hat{y}) = (x_{goal} \pm \epsilon, y_{goal} \pm \epsilon)$$

The robot will have an angular velocity as

$$\dot{\theta}_r = \alpha \cdot \arctan \left(\frac{v_x \cdot y_{goal} - v_y \cdot x_{goal}}{v_x \cdot x_{goal} + v_y \cdot y_{goal}} \right)$$

where v_x and v_y is the velocity of the robot in the x -axis and y -axis respectively, and α is a scaling constant. If the difference between the robot's and the target heading is greater than $\frac{\pi}{36}$ then the robot's linear speed is reduced to 0.1, allowing time to correct its course.

The collider's initial position is

$$(x, y, \theta) = (\mathcal{U}(-x_{lim}, x_{lim}), \mathcal{U}(0, y_{lim}), \mathcal{U}(-\pi, \pi))$$

where \mathcal{U} is the uniform distribution function. The collider's linear speed and angular speed were determined using the following function

$$(s, \dot{\theta}_c) = (\mathcal{U}(0, s_{lim}), \mathcal{U}(-\dot{\theta}_{lim}, \dot{\theta}_{lim}))$$

Table 1 provides the values used for the experimental setup.

Table 2: Hyperparameters for training DNN models

Hyperparameter	Collision Detection DNN	Driver Attentiveness Levels DNN
# of epochs	100	100
batch size	32	128
initial learning rate	0.005	0.01
optimizer	Adam	Adam
ϵ	0.05	0.01
τ	0.8	0.7

A collected datapoint was of the form $(x_{diff}, y_{diff}, s, \theta, \dot{\theta}_c, c)$, where x_{diff} and y_{diff} is the relative distance in the x and y axes between the robot and collider, and c is the label for collision/no collision. The datapoints were normalised for the DNN; [0,1] for y_{diff} and s and [-1,1] for x_{diff} , θ and $\dot{\theta}_c$.

The training data for the collision detection DNN was gathered through repeated simulations until 6×10^3 instances of collisions and 6×10^3 instances of no collisions occurred, with the collider's setup normalised and recorded. The time to complete a journey with a collision, and the time to complete without a collision was calculated from averages of 10×10^3 simulations for both collision and no collision instances. We used 80% of this dataset for training the DNN and 20% for calibration and validation. To gather the test dataset, 50×10^3 simulations were conducted which had a split of 5843 collisions and 44157 no collisions. This was passed through the trained DNN with the verification methods and the resultant confusion matrices were used to generate the model's probabilities of the DNN, see Figure 4a.

The dataset for the driver attentiveness management DNN was obtained from a user study²⁸ conducted as part of our SafeSCAD project. The data was normalised in the range [0,1]. We used 60% of the dataset for training the DNN and 15% for calibration and validation. The remaining 25% of the dataset was used for testing the DNN model and constructing the confusion matrices.

DNN training. The two autonomous systems considered in our evaluation, namely, a mobile robot navigation system and a system for maintenance of driver attentiveness level, use DNN-based classifiers for perception. In the first case, a DNN is used to detect if a mobile robot is on a collision path with another mobile robot in the second environment. In the second case, a DNN helps gauge a car driver's attentiveness levels.

The DNN for collision detection has the architecture prescribed by Ehlers²⁴ - the network has a fully-connected linear layer with 40 nodes, followed by a MaxPool layer with pool size 4 and stride size 1, followed by a fully-connected ReLU layer with 19 nodes, and a final fully-connected ReLU layer with 2 nodes. The DNN for gauging driver attentiveness level has an architecture with 10 layers, with eight fully-connected layers and two MaxPool layers (with additional Reshape layers as needed) . The 10 layers from start to end are as follows - fully-connected ReLU layer with 23 nodes, fully-connected ReLU layer with 50 nodes, fully-connected ReLU layer with 80 nodes, MaxPool layer with pool size 4 and stride size 1, fully-connected ReLU layer with 40 nodes, MaxPool layer with pool size 4 and stride size 1, fully-connected ReLU layer with 20 nodes, fully-connected ReLU layer with 14 nodes, fully-connected ReLU layer with 8 nodes, and a fully-connected linear layer with 3 nodes.

We train these models with a cross-entropy loss function (implicitly assuming a final softmax layer for both the DNNs) using the Adam optimization algorithm.⁴⁰ Table 2 lists the hyperparameters used for training the DNN models. Note that the learning rate in both cases is set to decay to 0.0001. We implement our DNN models and their training in Python, using TensorFlow.

DNN verification. We use DNN verifiers that check if a DNN satisfies specific properties of interest to augment a DNN’s outcome. For every input, in addition to the DNN’s prediction, the controller has access to the boolean outcomes of the DNN verifiers to aid in decision-making. As described in Section 1.3, we also use the DNN verification outcomes to construct fine-grained confusion matrices from the validation dataset. These confusion matrices help us compute empirical estimates of the probability of an incorrect prediction, conditioned on the correct prediction and the verification outcomes. These estimates are then used to synthesize a discrete-event controller that can account for the uncertainty in DNN predictions in it’s decision-making.

The specific DNN properties that we consider for verification are the local robustness of the DNN at an input, and the probability assigned by the DNN classifier to the predicted class. For local robustness verification, we use the GloRo Net framework of Leino et al.³⁰ Given a DNN, the GloRo Net framework adds a new final layer to the network that augments the DNN outcome with an additional outcome indicating the local robustness of the DNN. This new layer computes the Lipschitz constant of the function denoted by the original DNN and uses it to verify local robustness. Instead of training the original DNN, the GloRo Net framework recommends training the modified DNN to help improve the robustness of the network. We follow this recommendation for both the systems that we study, and update the DNN architectures described earlier by adding the layer provided by the GloRo Net framework as the final layer. For the collision detection DNN, we verify local robustness of the within radius $\epsilon=0.05$ (where ϵ is as defined in 4) whereas we use $\epsilon=0.01$ for the DNN that gauges driver attentiveness levels.

For verifying if the DNN predictions meets a minimum confidence threshold, we look at the softmax output of the DNN classifier that assigns a probability to each class. To ensure that the DNN softmax outputs are well-calibrated, we use the simple temperature scaling mechanism presented by Guo et al.¹² as implemented by Kueppers et al.⁴¹ We use the probability threshold τ of 0.8 for the collision detection DNN and threshold τ of 0.7 for the DNN that predicts driver attentiveness levels (where τ is as defined in 3).

SafeSCAD DNN-perception controller synthesis. The probabilistic model synthesis tool EvoChecker²⁰ was required for generating the Pareto fronts in the SafeSCAD study due to the large search space. For all setups the population size for the multi-objective genetic algorithm employed by EvoChecker was set to 1000 and the maximum number of evaluations was 20×10^4 . EvoChecker utilised the Viking Cluster (see here for full technical details <https://www.york.ac.uk/it-services/services/viking-computing-cluster/#tab-1>), and specifically used 5 CPUs and 8GB of memory, with a set maximum time of five hours.

Pareto front hypervolume evaluation. HV for both case studies was calculated using the package *PyGMO* (<https://esa.github.io/pygmo/>). For HV a nadir point is required, which is usually found via the extrema of the reference frame scaled by a constant. The Pareto fronts of the setup with the perfect DNN were used as the reference frames, with a scaling factor of 1.5 in the collision avoidance scenario and 1.75 for the SafeSCAD study.

PyGMO for HV calculation requires the system’s goal to minimise all objectives. Therefore for the collision avoidance scenario a Pareto front was generated to no longer maximise $\mathcal{P}_{=?}[\neg \text{collision} \wedge \text{done}]$ but instead minimise $\mathcal{P}_{=?}[\text{collision} \wedge \text{done}]$, i.e. maximise probability of being safe to minimise probability of being at risk. This was achieved by using the existing Pareto front and calculating the complementary probability; $1 - \mathcal{P}_{=?}[\neg \text{collision} \wedge \text{done}]$.

Validation of collision-mitigation controllers. The results presented in Figure 4d were achieved by first acquiring data buckets for setups resulting in collision and no collision. This was to ensure that the probability of encountering a collider that will result in collision in the model was replicated in the simulator. Simulations were conducted until 50×10^3 collision instances and 50×10^3 no collision instances were recorded. To ensure that these were guaranteed setups to achieve the desired result each setup was tested through 100 simulations to assure that the outcome was consistent. For the simulations producing the results in Figure 4d the setup for the collider (providing a collider was present determined by probability p_{collider}) used the weighted probability used in the model, p_{occ} see Figure 3. The robot used the trained DNN and verification methods to decide which parameter of the synthesised controller to use. If the robot decided to wait the wait time was added and the simulation restarted, i.e. the old collider was removed with a new collider. Once the robot had completed it’s journey the journey time was recorded along with whether a collision occurred. To compare with the model, the model’s results were subtracted from the simulator’s averaged values to acquire the difference plotted in Figure 4d.

Acknowledgements

This project has received funding from the UKRI project EP/V026747/1 ‘Trustworthy Autonomous Systems Node in Resilience’, the UKRI Global Research and Innovation Programme, and the Assuring Autonomy International Programme. The authors are grateful to the developers of the DeepTake deep neural network²⁸ for sharing the DeepTake data sets, and to the University of York’s Viking research computing cluster team for providing access to their systems.

References

- [1] Alvin I. Chen, Max L. Balter, Timothy J. Maguire, and Martin L. Yarmush. Deep learning robotic guidance for autonomous vascular access. *Nat Mach Intell*, 2:104–115, 2020.
- [2] Jeffrey De Fauw, Joseph R Ledsam, Bernardino Romera-Paredes, Stanislav Nikolov, Nenad Tomasev, Sam Blackwell, Harry Askham, Xavier Glorot, Brendan O’Donoghue, Daniel Visentin, et al. Clinically applicable deep learning for diagnosis and referral in retinal disease. *Nature medicine*, 24(9):1342–1350, 2018.
- [3] Thomas Fischer and Christopher Krauss. Deep learning with long short-term memory networks for financial market predictions. *European Journal of Operational Research*, 270(2):654–669, 2018.
- [4] Sorin Grigorescu, Bogdan Trasnea, Tiberiu Cocias, and Gigel Macesanu. A survey of deep learning techniques for autonomous driving. *Journal of Field Robotics*, 37(3):362–386, 2020.
- [5] Domen Tabernik and Danijel Skočaj. Deep learning for large-scale traffic-sign detection and recognition. *IEEE Transactions on Intelligent Transportation Systems*, 21(4):1427–1440, 2019.
- [6] Rob Ashmore, Radu Calinescu, and Colin Paterson. Assuring the machine learning lifecycle: Desiderata, methods, and challenges. *ACM Computing Surveys*, 54(5):1–39, 2021.
- [7] Vijay D’silva, Daniel Kroening, and Georg Weissenbacher. A survey of automated techniques for formal software verification.

IEEE Transactions on Computer-Aided Design of Integrated Circuits and Systems, 27(7):1165–1178, 2008.

[8] Guy Katz, Derek A Huang, Duligur Ibeling, Kyle Julian, Christopher Lazarus, Rachel Lim, Parth Shah, Shantanu Thakoor, Haoze Wu, Aleksandar Zeljić, et al. The Marabou framework for verification and analysis of deep neural networks. In *CAV*, pages 443–452. Springer, 2019.

[9] Xiaowei Huang, Marta Kwiatkowska, Sen Wang, and Min Wu. Safety verification of deep neural networks. In Rupak Majumdar and Viktor Kunčak, editors, *CAV*, pages 3–29, 2017.

[10] Divya Gopinath, Guy Katz, Corina S Păsăreanu, and Clark Barrett. DeepSafe: A data-driven approach for assessing robustness of neural networks. In *ATVA*, pages 3–19, 2018.

[11] On-Road Automated Driving (ORAD) committee. Taxonomy and definitions for terms related to driving automation systems for on-road motor vehicles. Standard J3016_201806, SAE International, 2018.

[12] Chuan Guo, Geoff Pleiss, Yu Sun, and Kilian Q. Weinberger. On calibration of modern neural networks. In *Proceedings of the 34th International Conference on Machine Learning - Volume 70*, ICML17, page 1321–1330. JMLR.org, 2017.

[13] Nicholas Carlini and David Wagner. Towards evaluating the robustness of neural networks. In *2017 IEEE Symposium on Security and Privacy*, pages 39–57. IEEE, 2017.

[14] Conrado Daws. Symbolic and parametric model checking of discrete-time Markov chains. In *International Colloquium on Theoretical Aspects of Computing*, pages 280–294, 2005.

[15] Hans Hansson and Bengt Jonsson. A logic for reasoning about time and reliability. *Formal Aspects of Computing*, 6(5):512–535, 1994.

[16] Andrea Bianco and Luca De Alfaro. Model checking of probabilistic and nondeterministic systems. In *International Conference on Foundations of Software Technology and Theoretical Computer Science*, pages 499–513. Springer, 1995.

[17] Suzana Andova, Holger Hermanns, and Joost-Pieter Katoen. Discrete-time rewards model-checked. In *International Conference on Formal Modeling and Analysis of Timed Systems*, pages 88–104. Springer, 2003.

[18] Marta Kwiatkowska, Gethin Norman, and David Parker. PRISM 4.0: Verification of probabilistic real-time systems. In *Proc. of the 23rd Int. Conf. on Computer Aided Verification*, volume 6806 of *LNCS*, pages 585–591. Springer, 2011.

[19] Radu Calinescu, Milan Ceska, Simos Gerasimou, Marta Kwiatkowska, and Nicola Paoletti. Efficient synthesis of robust models for stochastic systems. *Journal of Systems and Software*, 143:140 – 158, 2018.

[20] Simos Gerasimou, Radu Calinescu, and Giordano Tamburrelli. Synthesis of probabilistic models for quality-of-service software engineering. *Automated Software Engineering*, 25(4):785–831, 2018.

[21] Kyle D Julian, Mykel J Kochenderfer, and Michael P Owen. Deep neural network compression for aircraft collision avoidance systems. *Journal of Guidance, Control, and Dynamics*, 42(3):598–608, 2019.

[22] Kyle D Julian and Mykel J Kochenderfer. Reachability analysis for neural network aircraft collision avoidance systems. *Journal of Guidance, Control, and Dynamics*, 44(6):1132–1142, 2021.

[23] Qingyang Xu, Yiqin Yang, Chengjin Zhang, and Li Zhang. Deep convolutional neural network-based autonomous marine vehicle maneuver. *International Journal of Fuzzy Systems*, 20(2):687–699, 2018.

[24] Rüdiger Ehlers. Formal verification of piece-wise linear feed-forward neural networks. In Deepak D’Souza and K. Narayan Kumar, editors, *Automated Technology for Verification and Analysis*, pages 269–286. Springer, 2017.

[25] David A. Van Veldhuizen. *Multiobjective evolutionary algorithms: classifications, analyses, and new innovations*. PhD thesis, Ph. D. thesis, 1999.

[26] Eckart Zitzler and Lothar Thiele. Multiobjective evolutionary algorithms: a comparative case study and the strength pareto approach. *IEEE transactions on Evolutionary Computation*, 3(4):257–271, 1999.

[27] UNECE. ECE/TRANS/WP.29/2020/81—United Nations Regulation on Uniform provisions concerning the approval of vehicles with regard to Automated Lane Keeping Systems, June 2020.

[28] Erfan Pakdamanian, Shili Sheng, Sonia Bae, Seongkook Heo, Sarit Kraus, and Lu Feng. DeepTake: Prediction of driver takeover behavior using multimodal data. In *2021 CHI Conference on Human Factors in Computing Systems*, pages 1–14, 2021.

[29] Radu Calinescu, Naif Alasmari, and Mario Gleirscher. Maintaining driver attentiveness in shared-control autonomous driving. In *16th International Symposium on Software Engineering for Adaptive and Self-Managing Systems*, pages 90–96. IEEE, 2021.

[30] Klas Leino, Zifan Wang, and Matt Fredrikson. Globally-robust neural networks. In *International Conference on Machine Learning (ICML)*, 2021.

[31] Colin Paterson, Radu Calinescu, and Chiara Picardi. Detection and mitigation of rare subclasses in deep neural network classifiers. In *2021 IEEE International Conference on Artificial Intelligence Testing*, pages 9–16. IEEE, 2021.

[32] Gagandeep Singh, Timon Gehr, Markus Püschel, and Martin Vechev. An abstract domain for certifying neural networks. *Proc. ACM Program. Lang.*, 3(POPL), jan 2019.

[33] Susmit Jha, Vasumathi Raman, Dorsa Sadigh, and Sanjit A. Seshia. Safe autonomy under perception uncertainty using chance-constrained temporal logic. *Journal of Automated Reasoning*, 60(1):43–62, 2018.

[34] Rhiannon Michelmore, Matthew Wicker, Luca Laurenti, Luca Cardelli, Yarin Gal, and Marta Kwiatkowska. Uncertainty quantification with statistical guarantees in end-to-end autonomous driving control. In *2020 IEEE International Conference on Robotics and Automation (ICRA)*, pages 7344–7350, 2020.

[35] Matthew Cleaveland, Ivan Ruchkin, Oleg Sokolsky, and Insup Lee. Monotonic safety for scalable and data-efficient probabilistic safety analysis, 2021.

[36] Edwin Fong and Christopher C. Holmes. Conformal bayesian computation. In *Thirty-Fifth Conference on Neural Information Processing Systems*, 2021.

[37] Volodya Vovk, Alexander Gammerman, and Craig Saunders. Machine-learning applications of algorithmic randomness. In *Proceedings of the Sixteenth International Conference on Machine Learning*, pages 444–453, 1999.

[38] Vladimir Vovk, Alexander Gammerman, and Glenn Shafer. *Algorithmic learning in a random world*. Springer Science & Business Media, 2005.

- [39] Stephen Bates, Anastasios Angelopoulos, Lihua Lei, Jitendra Malik, and Michael Jordan. Distribution-free, risk-controlling prediction sets. *J. ACM*, 68(6), September 2021.
- [40] Diederik P. Kingma and Jimmy Ba. Adam: A method for stochastic optimization. In Yoshua Bengio and Yann LeCun, editors, *3rd International Conference on Learning Representations, ICLR 2015, San Diego, CA, USA, May 7-9, 2015, Conference Track Proceedings*, 2015.
- [41] Fabian Küppers, Jan Kronenberger, Amirhossein Shantia, and Anselm Haselhoff. Multivariate confidence calibration for object detection. In *The IEEE/CVF Conference on Computer Vision and Pattern Recognition (CVPR) Workshops*, June 2020.